JOURNAL OF ENZYME INHIBITION AND MEDICINAL CHEMISTRY
2023, VOL. 38, NO. 1, 2166037
https://doi.org/10.1080/14756366.2023.2166037

Taylor & Francis
Taylor & Francis Group

RESEARCH PAPER

Identification of new benzimidazole-triazole hybrids as anticancer agents: multi-target recognition, *in vitro* and *in silico* studies

Dina I. A. Othman[a], Abdelrahman Hamdi[a], Samar S. Tawfik[a], Abdullah A. Elgazar[b] and Amany S. Mostafa[a]

[a]Department of Pharmaceutical Organic Chemistry, Faculty of Pharmacy, Mansoura University, Mansoura, Egypt; [b]Department of Pharmacognosy, Faculty of Pharmacy, Kafrelsheikh University, Kafrelsheikh, Egypt

ABSTRACT

Multi-target inhibitors represent useful anticancer agents with superior therapeutic attributes. Here in, two novel series of benzimidazole-triazole hybrids were designed, synthesised as multi-target EGFR, VEGFR-2 and Topo II inhibitors, and evaluated for anticancer activity. Compounds **5a** and **6g** were the most potent analogues against four cancer cell lines, HepG-2, HCT-116, MCF-7 and HeLa, and were further evaluated for EGFR, VEGFR-2, and Topo II inhibition. Compound **5a** was especially good inhibitor for EGFR ($IC_{50} = 0.086\,\mu M$) compared to Gefitinib ($IC_{50} = 0.052\,\mu M$), moderate VEGFR-2 inhibitor ($IC_{50} = 0.107\,\mu M$) compared to Sorafenib ($IC_{50} = 0.0482\,\mu M$), and stronger Topo II inhibitor ($IC_{50} = 2.52\,\mu M$) than Doxorubicin ($IC_{50} = 3.62\,\mu M$). Compound **6g** exhibited moderate EGFR and VEGFR-2 inhibition and weaker Topo II inhibition. DNA binding assay, cell cycle analysis, apoptotic induction, molecular docking, and physicochemical studies were additionally implemented to explore the plausible mechanism of the active compounds.

ARTICLE HISTORY
Received 23 October 2022
Revised 12 December 2022
Accepted 3 January 2023

KEYWORDS
Benzimidazole; 123-triazole hybrids; anticancer; EGFR; VEGFR-2; Topo II; molecular docking

GRAPHICAL ABSTRACT

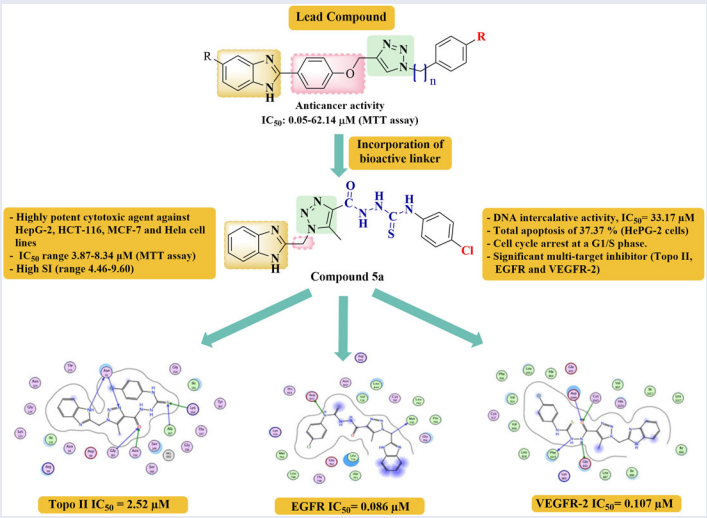

Introduction

Cancer is regarded as one of the most dreadful diseases worldwide. Development of more efficient drugs with multiple mechanisms became indispensable to control various cancer types, especially with the current innate ability of most cancer cells to evade the majority of the present chemotherapeutics[1–3]. Multi-targeting approaches give an ideal therapeutic paradigm to simultaneously interrupt more than one target to avoid prevailing drug resistance, giving insights for medicinal chemists to devote much effort for the design of new multi-targeted anticancer agents[4].

Benzimidazole nucleus appeared as a crucial pharmacophore in cancer research; owing to its diverse anticancer potential with versatile mechanisms of tumour inhibition, beside its facile synthetic strategies to get assorted derivatives[2–9]. Many reported anticancer drugs as well as different bioactive molecules contain the benzimidazole motif[10–15]. It was manifested that the anticancer potential and selectivity of benzimidazole derivatives depended radically on different substitutions comprised by the benzimidazole scaffold[2]. This was the promising master key that unlocked all the doors for the development of novel target-specific and highly effective benzimidazole-based anticancer agents. In particular, 2-substituted

CONTACT Amany S. Mostafa amanysalah2002@yahoo.com Department of Pharmaceutical Organic Chemistry, Faculty of Pharmacy, Mansoura University, Mansoura, Egypt

Supplemental data for this article can be accessed online at https://doi.org/10.1080/14756366.2023.2166037.

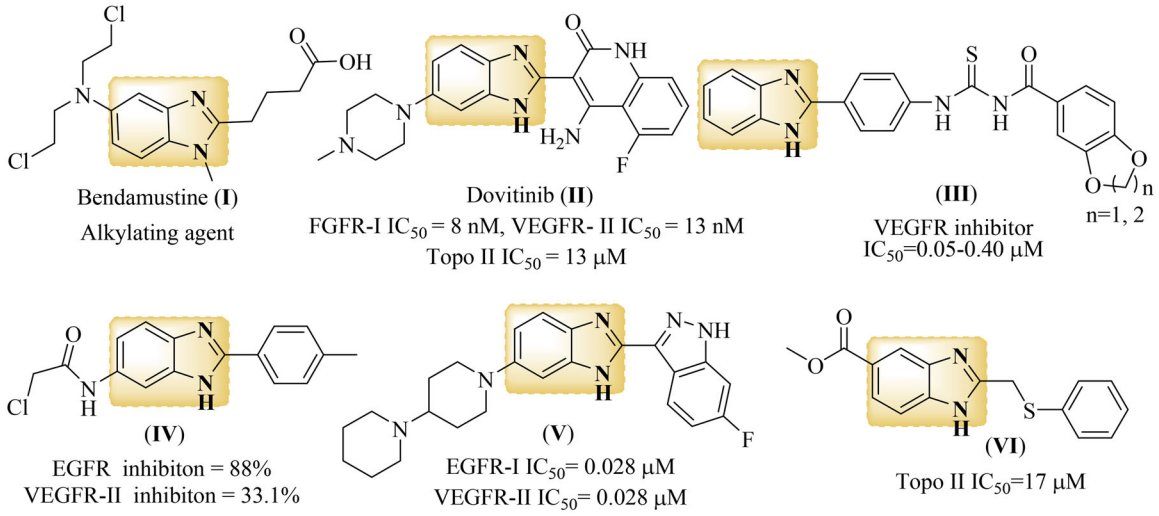

Figure 1. Reported 2-substituted benzimidazoles as multi-target enzyme inhibitors.

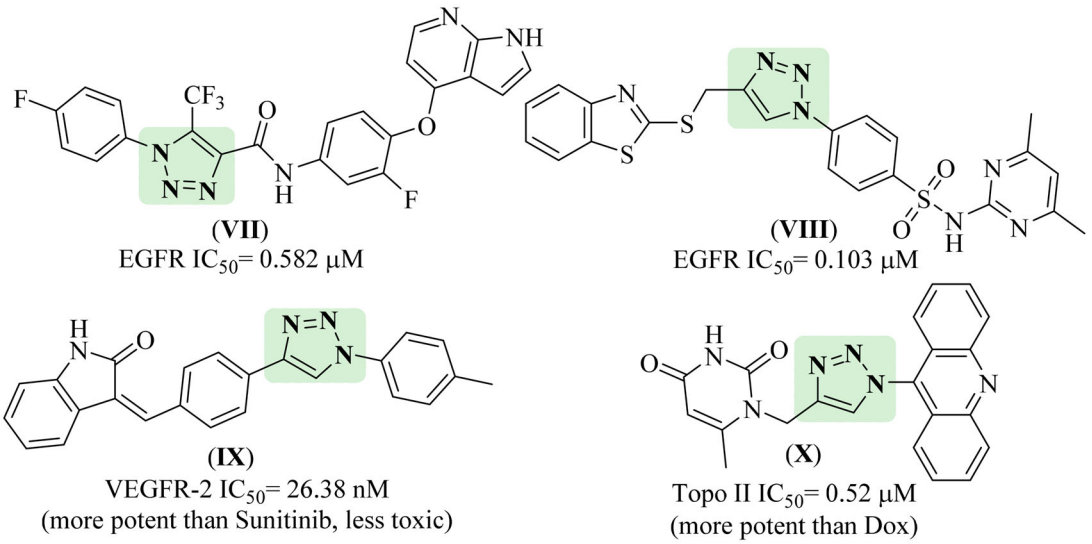

Figure 2. Reported 1,2,3-triazole scaffolds as multi-target enzyme inhibitors.

benzimidazoles have been widely explored as anticancer agents with unique mechanisms, targeting not only different tyrosine kinases, but also other enzymes[5,6].

As shown in Figure 1, Bendamustine (**I**) is a nitrogen mustard benzimidazole based alkylating agent used in the treatment of chronic lymphoma[6]. Dovitinib (**II**) is an orally active benzimidazole-quinolinone hybrid with potential antineoplastic activity as multiple receptor tyrosine kinases' (RTKs) inhibitor. It strongly targets fibroblast growth factor receptor-1 (FGFR-1) ($IC_{50} = 8$ nM), vascular endothelial growth factor receptor-2 (VEGFR-2) ($IC_{50} = 13$ nM), and other RTKs involved in tumour growth and angiogenesis, like FGFR-3, VEGFR-1, VEGFR-3, and PDGFR. It also targets Topoisomerase II (Topo II) enzyme with IC_{50} of 13 μM[8]. Dovitinib has been exclusively in-licensed worldwide by Novartis, who has completed phase-III study against renal cell carcinoma (RCC), in addition to several promising phase-II studies against liver, breast, endometrial cancer, and gastrointestinal stromal tumour[10–12].

Further, 2-substituted benzimidazole analogues (**III**) were assessed for their antitumor and antiangiogenic activities. They effectively antagonised VEGF-A165/NRP-1 binding, with IC_{50} values range of 0.05–0.40 μM[13]. In addition, a new series of 2-aryl benzimidazoles was designed as multi-target RTKs inhibitors, and biologically evaluated against HepG-2 cells and different kinases; where compound (**IV**) gave 88% inhibition of epidermal growth factor receptor (EGFR), 33.1% inhibition of VEGFR-2, and a range of 42.7–52.6% inhibition concerning platelet-derived growth factor receptors (PDGFR-α,β)[6]. Likewise, 2,5-disubstituted benzimidazole-indazole hybrids were designed and synthesised as multi-inhibitors of VEGFR-1, VEGFR-2, PDGFR, and FGFR-1, where compound (**V**) afforded potent effect against all the tested RTKs, with favourable pharmacokinetics and improved *in vivo* tumour growth inhibition properties that reached to about 88%[13].

Moreover, other 2-substituted benzimidazole derivatives were identified as potent Topo II inhibitors[15,16], like the 2-phenylthiomethylbenzimidazole (**VI**) that displayed enhanced activity against Topo II with IC_{50} of 17 μM, which is more potent than Etoposide reference drug ($IC_{50} = 21.8$ μM)[15].

On the other hand, 1,2,3-triazole motifs have recently received considerable attention in drug discovery for the development of novel anticancer agents, since they represented potent pharmacophores that are implicated in numerous anticancer compounds[17,18]. They have been reported to exert outstanding anticancer effect through different mechanisms *via* inhibition of various enzymes (Figure 2)[17,18]. Triazole scaffold (**VII**) showed

significant *in vitro* cytotoxicity against different human cancer cell lines *via* remarkable kinase inhibitory activity against EGFR ($IC_{50} = 0.582\ \mu M$)[19]. Similarly, the triazole derivative (**VIII**) offered potent inhibitory activity against EGFR ($IC_{50} = 0.103\ \mu M$), compared to Erlotinib. The docking study revealed similar interactions with Erlotinib in the specified binding pocket, confirming its role as EGFR inhibitor. It formed a hydrogen bond with the Met769 amino acid residue *via* the triazole N3, in addition to double aromatic stabilisation with both Gly772 and Leu694 residues in the hinge region. Furthermore, the benzothiazole ring; that is considered to be a structural isostere of benzimidazole; presented good interaction with Leu820 and Asp831 key residues[18].

An indole-2-one-based 1,2,3-triazole scaffold (**IX**) has displayed significant VEGFR inhibition on cancer cells ($IC_{50} = 26.38$ nM, better than Sunitinib, $IC_{50} = 83.20$ nM) whereas it was less toxic to human cells[20]. Furthermore, the docking studies of this scaffold confirmed that it is spatially embedded in a perfect way within the protein binding pocket, leading to potential VEGFR-2 inhibition[20]. Besides, the triazole derivative (**X**) displayed greater inhibitory activity against Topo IIB ($IC_{50} = 0.52\ \mu M$) compared with Doxorubicin (Dox) ($IC_{50} = 0.83\ \mu M$)[21].

Accordingly, the attachment of the well reported anticancer pharmacophores; 2-substituted benzimidazole along with a 1,2,3-triazole backbone, based on a hybrid pharmacophore design, became an encouraging strategy to develop new highly effective anticancer candidates against both drug-resistant and drug-sensitive cancers due to their expected combined mechanisms. Over the past few years, benzimidazole-1,2,3-triazole hybrids (**XI**) were verified to exhibit considerable activity against A549, HeLa, CFPAC-1 (ductal pancreatic adenocarcinoma), and SW620 (metastatic colorectal adenocarcinoma) cells, with IC_{50} range of 0.05–62.14 μM, using MTT assay, where some compounds showed activity comparable to or even better than 5-Fluorouracil (IC_{50} range of 0.08–8.81), depending on certain variables[22,23]. Structure-activity relationship (SAR) studies suggested that the shorter carbon spacer between 1,2,3-triazole and benzimidazole moiety was favourable to the activity, whereas the longer side chain between 1,2,3-triazole and other motifs was preferred[22–24].

Thus, taking together all these findings, we envisioned that a hybrid approach that combines benzimidazole at position 2 with 1,2,3-triazole *via* short ($-CH_2$) group spacer unit, and using different elongated linkers between the triazole nucleus and other motifs in one structure might provide a new hybrid scaffold (**XII**) with potentiated multi-targeted; EGFR, VEGFR-2, and Topo II inhibitory activities (Figure 3). Moreover, it was reported in different studies that the embodiment of (thio)ureido-moiety, like that present in Tivozanib, Sorafenib, and compound **XIII**, or azomethine connecting group, as in compound **XIV**, within the structure of a given compound, could enhance the antitumor activity[3,25,26]. Therefore, our new scaffold (**XII**) was diversified by incorporating

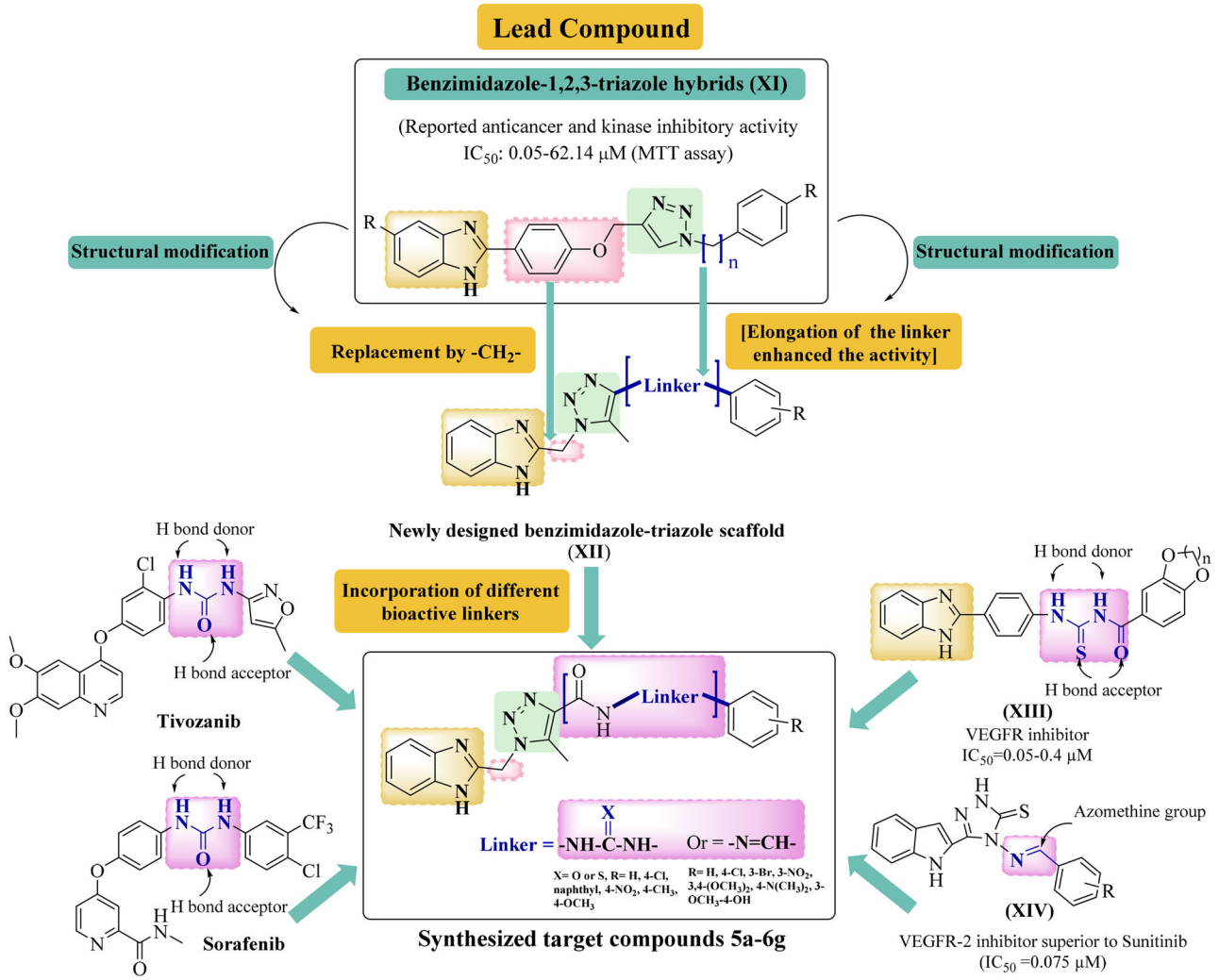

Figure 3. Rational design of the newly synthesised benzimidazole-triazole hybrids.

these active linkers as long spacers between 1,2,3-triazole and the aryl motif, hoping to get more potent anticancer candidates with multi-targeted molecular mechanisms (Figure 3). On the other hand, connecting various substituents of different electronic properties to the phenyl ring was also accomplished, to explore their impact on activity. In brief; the rational design of our new compounds was based on the following considerations: (i) the benzimidazole scaffold itself, (ii) the presence of the effective 2-substituted position, (iii) linking of 1,2,3-triazole nucleus to the benzimidazole entity through short CH_2- connecting group, which seems to play a crucial role in the cytotoxic activity, (iv) employing varied long spacers between the 1,2,3-triazole and different substituted phenyl rings to examine their cytotoxic behaviour, as shown in Figure 3, and (v) investigate the chemical nature of different moieties and their hydrogen bond acceptor or donor properties, enclosed in the structures of the designed target compounds, which may contribute to the tolerability of these compounds within the binding pockets of targeted enzymes. Hopefully, our target compounds were designed to embrace the common structural requirements that can adequately fit with the three intended target enzymes; EGFR, VEGFR 2, and Topo II. The involvement of triazole ring was guaranteed to form the reported hydrogen bond with the Met793 amino acid residue, which is an essential feature for EGFR inhibition[19]. Further, all compounds contain the hydrogen bond domain and the hydrophobic tail, which are essential requirements for VEGFR 2 binding, like (thio)urea, or azomethine linkers[3,25,26]. Moreover, the presence of benzimidazole nucleus in all derivatives was adopted as an essential scaffold for Topo II inhibition, where the benzimidazole nitrogen is reported to bind with the essential amino acid residues needed for activity, like Asn120, Asn95, Asn91, As150, Arg98, Ser148, or Lys157[15,16].

Herein, we report our fruitful findings on the synthesis, characterisation and *in vitro* pharmacological evaluation of new series of benzimidazole-triazole hybrids, with different linkers, in order to produce potential multi-targeting anti-proliferative candidates. In an attempt to reveal the anticipated antitumor mechanism, cell cycle analysis beside EGFR, VEGFR-2, and Topo II inhibitory activities have been evaluated. Furthermore, molecular docking and physicochemical studies were assessed.

Results and discussion

Chemistry

The synthetic route used to access our target compounds **5a–h** and **6a–g** is shown in Scheme 1. 2-Chloro methyl benzimidazole **1** was transformed into the corresponding azide **2**, using sodium azide in dry DMSO[23]. Then, the formed azide **2** was condensed with ethyl acetoacetate (EAA) to afford the intermediate ester **3**, which was further reacted with hydrazine hydrate to give the corresponding hydrazide **4**[27,28]. The final target compounds **5a–h** were obtained by reacting the hydrazide **4** with the appropriate substituted iso(thio)cyanates in THF at room temperature overnight. While compounds **6a–g** were attained by reacting the hydrazide **4** with various benzaldehyde derivatives in refluxing ethanol, in the

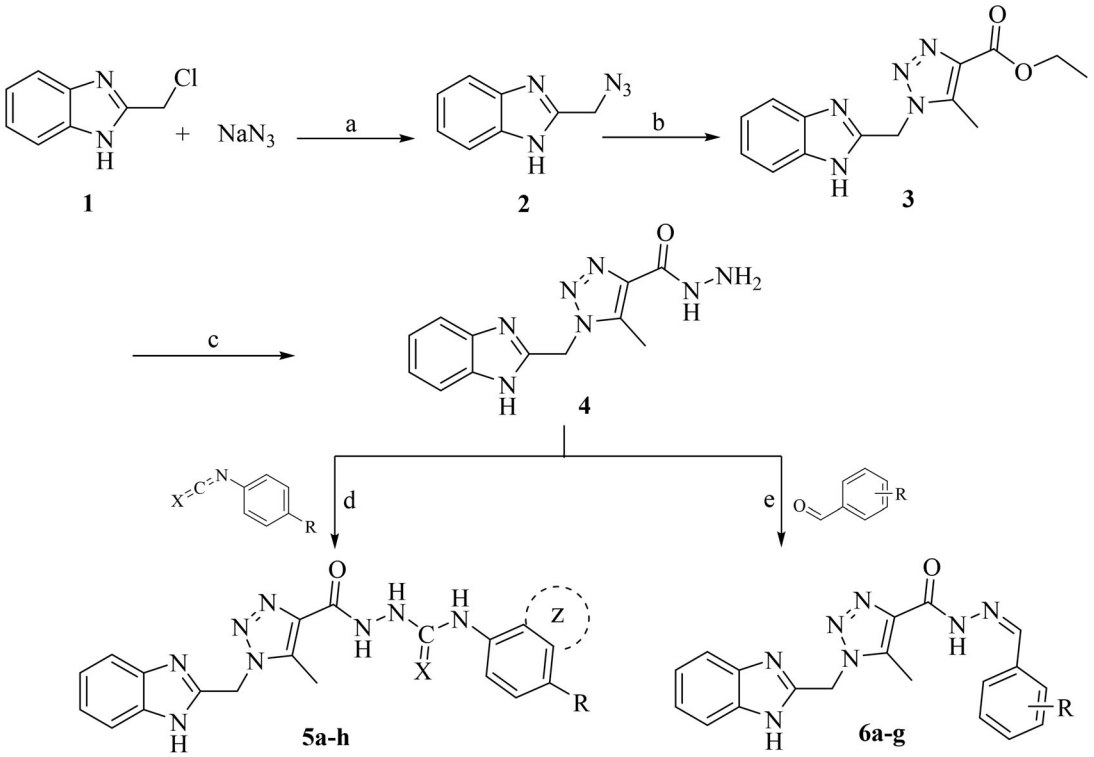

Scheme 1. Reagents and conditions: (a) DMSO, stirring, rt, 15 h, (b) EAA, K_2CO_3, DMSO, stirring, rt, overnight, (c) $NH_2NH_2.H_2O$, EtOH, stirring, rt, overnight, (d) THF, stirring, rt, (e) EtOH, AcOH, reflux

presence of catalytic amount of glacial acetic acid. The structures of all the title compounds were confirmed by IR, ^{1}H-NMR, ^{13}C-APT NMR, and elemental analysis. The ^{1}H-NMR spectra of all synthesised target compounds were characterised by the disappearance of distinctive NH_2 signal, formerly appearing at 4.45 ppm in the spectrum of the starting hydrazide **4**. In addition, two characteristic singlet signals appeared in all compounds, at ~ 2.64 and 5.94 ppm, corresponding to methyl protons (-CH_3) and methylene protons (-C$\underline{CH_2}$N-), respectively. The formation of carbothio(oxa)amide derivatives **5a-h** was also confirmed by the presence of remarkable singlet peaks, that appeared downfield in the range of 8.20–10.50 ppm, referring to the exchangeable NH protons (-$\underline{NH}$N$\underline{H}$CX$\underline{NH}$-); while the formation of arylidene derivatives **6a-g** was confirmed by the presence of characteristic singlet peak at ~ 8.60 ppm, that corresponds to the azo methine proton (-N=$\underline{CH}$-). Furthermore, ^{13}C-APT NMR spectra revealed the appearance of two peaks at ~157.0–163.0 ppm in compounds **5a-h**, related to carbonyl/thione carbons or one peak at ~157.5 ppm in derivatives **6a-g**, related to carbonyl carbon. In addition, all final targets showed two characteristic peaks in the aliphatic region at approximately 8.9–45.9 ppm that were corresponded to the methyl and methylene carbons. All other spectral and analytical data were consistent with the assumed structures. The mass spectra of the final targets showed the correct molecular ion peaks (M^{+}), as suggested by their molecular formulas. All compounds gave good CHNS quantitative elemental analysis results, in agreement with the calculated values.

Biological activity

In vitro studies

In vitro *cytotoxic study against HepG-2, HCT-116, MCF-7, and HeLa cell lines.* The newly synthesised compounds were screened for their cytotoxic activity against hepatocellular carcinoma (HepG-2), human colon carcinoma (HCT-116), breast adenocarcinoma (MCF-7), and cervical cell carcinoma (HeLa) at various concentrations *via* the standard MTT assay method, using Dox as a reference drug (Table 1). Inspection of results denoted that compounds **5a** and **6g** showed very strong cytotoxic activity against all the tested cancer cell lines. Within the first series **(5a-h)**, compound **5g** displayed very strong activity against HeLa and MCF-7 cells with IC_{50} values of 8.70 and 9.39 μM, respectively, and strong effect against HepG-2 and HCT-116 with IC_{50} values of 13.59 and 18.67 μM, respectively. Besides, compound **5e** revealed strong activity against MCF-7 and HeLa cells with IC_{50} values of 16.57 and 19.14 μM, in succession, but gave moderate activity against HepG-2 and HCT-116. Compound **5d** exhibited strong HeLa cell cytotoxic activity with IC_{50} = 12.39 μM, whereas it showed moderate activity against HCT-116 and MCF-7 and weak inhibitory effect against HepG-2. Concerning the second series (**6a-g**), compound **6f** exhibited strong activity against HCT-116, MCF-7, and HepG-2 with IC_{50} values of 11.72, 14.69, and 18.31 μM, respectively, whereas it presented moderate activity against HeLa cells with IC_{50} = 22.75 μM. Also, compound **6e** exerted strong cytotoxic activity against HCT-116 with IC_{50} = 19.69 μM, but gave only moderate activity against MCF-7, HeLa, and HepG-2 cells with IC_{50} values of, 23.73, 29.07, and 33.62 μM, respectively. Derivative **6a** offered moderate activity towards the four tested cell lines, with IC_{50} range of 28.18–47.04 μM. Depending on the *in vitro* cytotoxic study, the tested compounds could be classified into four categories, ranging from weak to very strong active compounds, as shown in Table 1.

SAR analysis. SAR analysis of the antitumor activity of the newly synthesised compounds against HepG-2, HCT-116, MCF-7, and HeLa cells revealed that the length of the designed spacer has an impact upon activity, where the first series **5a-h**, having carbothio(oxa)amide moiety as a longer linker, providing 5-atom spacer,

Table 1. IC_{50} values (μM) of target compounds **5a-h** and **6a-g** against four cancer cell lines in comparison with Dox.

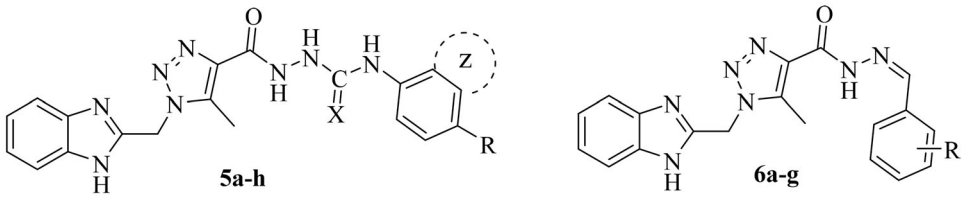

Comp. no.	R / Z	X	*In vitro* Cytotoxicity IC_{50} (μM)[a] HepG-2	HCT-116	MCF-7	HeLa
5a	Cl / –	S	**7.68 ± 0.5**	**8.34 ± 0.6**	**6.81 ± 0.4**	**3.87 ± 0.2**
5b	Cl / –	O	53.60 ± 2.9	37.69 ± 2.6	21.61 ± 1.9	46.20 ± 2.7
5c	H / Phenyl	O	67.42 ± 3.5	59.23 ± 3.3	45.35 ± 2.9	27.63 ± 2.0
5d	H / –	S	57.23 ± 3.2	41.38 ± 2.8	30.78 ± 2.3	12.39 ± 0.9
5e	NO_2 / –	O	25.03 ± 1.9	32.75 ± 2.4	16.57 ± 1.4	19.14 ± 1.4
5f	CH_3 / –	S	72.65 ± 3.8	68.45 ± 3.7	64.12 ± 3.3	58.15 ± 3.1
5g	OCH_3 / –	S	13.59 ± 1.0	18.67 ± 1.5	**9.39 ± 0.8**	**8.70 ± 0.6**
5h	H / –	O	42.14 ± 2.7	54.81 ± 3.0	38.02 ± 2.6	31.56 ± 2.3
6a	4-Cl	–	47.04 ± 2.8	28.18 ± 2.5	39.52 ± 2.6	35.33 ± 2.5
6b	H	–	84.46 ± 4.1	75.09 ± 3.8	57.56 ± 3.3	61.23 ± 3.4
6c	3-Br	–	56.28 ± 3.2	63.60 ± 3.3	44.81 ± 2.9	48.79 ± 2.8
6d	3-NO_2	–	71.50 ± 3.6	36.45 ± 2.7	48.25 ± 3.0	52.16 ± 3.1
6e	3,4-$(OCH_3)_2$	–	33.62 ± 2.3	19.69 ± 1.7	23.73 ± 1.9	29.07 ± 2.3
6f	4-$N(CH_3)_2$	–	18.31 ± 1.5	11.72 ± 0.9	14.69 ± 1.1	22.75 ± 1.9
6g	4-OH, 3-OCH_3	–	**10.92 ± 0.8**	**3.34 ± 0.4**	**7.11 ± 0.5**	**9.84 ± 0.7**
Dox[b]	–	–	4.50 ± 0.2	5.23 ± 0.3	4.17 ± 0.2	5.57 ± 0.4

[a]IC_{50} value is the concentration of compound that inhibits 50% of the cancer cell growth after 48 h of drug exposure as obtained from MTT assay. Each value was shown as mean ± SD of three independent experiments. IC_{50}, (μM): 1–10 (very strong), 11–20 (strong), 21–50 (moderate), 51–100 (weak), and above 100 (non-cytotoxic).

[b]Dox: Doxorubicin, used as reference drug. Bolded values represent the most potent anticancer derivatives.

showed slightly better activity to those of the benzylidene derivatives **6a-g**, that comprised 4-atom spacer.

Concerning the first carbothio(oxa)amide series **5a-h**, results demonstrated that most of compounds containing thiourea moiety exhibited more powerful antitumor activity than those incorporating urea moiety.

- Within the thiourea derivatives, it was deduced that the 4-chloro substitution in the aryl part gave the most potent compound **5a** against all the tested cell lines. Besides, the 4-methoxyphenyl substituted compound **5g** gave enhanced activity against both MCF-7 and HeLa cell lines. On the other hand, it was found that unsubstituted phenyl ring in compound **5d** affected the activity that was reported to be exclusively strong against HeLa. The methyl-substituted compound **5f** reported the least activity.
- Regarding the urea-containing derivatives, the effect of various substituents was also investigated, where either aryl unsubstitution in **5h**, 4-chlorosubstitution in **5b**, or even replacement of the phenyl ring with a naphthyl one in **5c** led to weak to moderate cytotoxic activity, while the 4-nitro-substituted compound **5e** has revealed strong activity against MCF-7 and HeLa cells.

Concerning the second series, representing the arylidene derivatives **6a-g**, it was detected that the presence of electron donating groups; like 3,4-dimethoxy, 4-dimethyl amino or 4-hydroxy, 3-methoxy groups; has notably enhanced the antitumor activity in compounds **6e-g**, compared to either unsubstituted aryl derivative **6b**, or those substituted with electron withdrawing groups; namely 4-chloro, 3-bromo, or 3-nitro groups like compounds **6a**, **6c**, and **6d**. Compounds **6e-g** displayed activity ranging from moderate to very strong activity. The dimethoxy derivative **6e** exhibited moderate effect against HepG-2, MCF-7, and HeLa cell, whereas it showed strong effect against HCT-116. Compound **6f** with the dimethyl amino-substitution also gave a moderate activity against HeLa cells, but was strongly active against the other three cell lines. The best activity in this series was obtained from the 4-hydroxy-3-methoxybenzylidene derivative **6g**, which showed very strong cytotoxic activity against all the four cell lines.

In vitro *cytotoxic activity of the most active compounds 5a and 6g against WI-38 cell line.* Normal Caucasian fibroblast-like foetal lung cells (WI-38) were used for further investigation of the cytotoxic effect and the therapeutic safety of the two new hybrids **5a** and **6g**, having the highest potency against the formerly tested cancer cell lines. Dox was used as a standard anticancer drug for comparison. Both compounds **5a** and **6g** exhibited lower cytotoxicity against WI-38 cells with IC_{50} values of 37.16 and 43.28 μM, respectively, in addition to more improved selectivity indexes (**SI**), proving to be much safer on normal cells compared to Dox ($IC_{50} = 6.72$ μM) (Table 2).

Table 2. *In vitro* cytotoxic study of the most active compounds 5a and 6g against WI-38 cell line and their selectivity indexes.

Comp.	Normal cells IC_{50} (μM) WI-38	SI[a] HepG-2	HCT-116	MCF-7	HeLa
5a	37.16 ± 2.4	4.73	4.46	5.46	9.60
6g	43.28 ± 2.6	4.2	12.95	6.09	4.39
Dox	6.72 ± 0.5	1.49	1.28	1.61	1.2

[a]SI: Selectivity Index = IC_{50} for normal cells/IC_{50} for cancer cells.

In vitro *enzyme inhibition assays.* The effect of compounds **5a** and **6g** was screened against several molecular targets, namely: EGFR, VEGFR-2, and Topo II. Both compounds expressed reasonable inhibitory activity against the three enzymes, compared to the specified reference drugs (Table 3).

The new hybrid **5a** showed remarkable inhibitory activity against EGFR with $IC_{50} = 0.086$ μM, that represented about 60% of activity of the reference drug Gefitinib ($IC_{50} = 0.052$ μM). Concerning VEGFR-2, compound **5a** gave about 45% of the inhibitory activity of Sorafenib. It is of much interest that it further displayed strong Topo II inhibitory activity with IC_{50} of 2.52 μM, which is superior to that of the reference drug Dox ($IC_{50} = 3.62$ μM) by about 1.4 folds.

Referring to compound **6g**, it conferred about 43% of activity of Dox towards Topo II, 40% of activity of Gefitinib against EGFR, while it was only 21% as potent as Sorafenib against VEGFR-2.

DNA binding activity assay

Several anticancer agents exert their effect throughout binding with DNA, and consequently inhibiting its synthesis. To assess the impact of the synthesised compounds on DNA binding properties, the most potent derivatives 5a and 6g were further evaluated for their DNA intercalating affinities, to be investigated as a potential mechanism for their anti-proliferative activities, using methyl green dye according to the reported technique[29]. Displacement of methyl green, ionically bound to DNA by the drug has been suggested as a potential assay for drug-DNA interaction[29]. As depicted in Table 4, the DNA binding results displayed that compound 5a exhibited nearly similar intercalative activity ($IC_{50} = 33.17$ μM) as Dox ($IC_{50} = 31.54$ μM). In addition, compound 6g showed DNA-binding activity with IC_{50} value of 42.03 μM. It is worthy noted that binding of these compounds to DNA can cause distortion of DNA helical structure, that leads to inhibition of its replication, transcription, and recombination, indicating that these compounds may act by such mechanism to attain their anticancer potential.

Cell cycle analysis

In order to gain more information regarding the mechanism of compounds **5a** and **6g** in growth inhibition of cancer cells, cell cycle distribution and induction of apoptosis on HepG-2 cells were evaluated using propidium iodide (PI) staining assay[30,31]. The obtained results (Table 5 and Figure 4**)** indicated that compounds

Table 3. *In vitro* EGFR-2, VEGFR-2, and Topo II inhibitory effects of the synthesised compounds 5a and 6g compared to reference drugs.

Compound	EGFR IC_{50} (mean ± SD μM)	VEGFR-2 IC_{50} (mean ± SD μM)	Topo II IC_{50} (mean ± SD μM)
5a	0.086 ± 0.009	0.107 ± 0.005	2.52 ± 0.15
6g	0.131 ± 0.005	0.229 ± 0.01	8.37 ± 0.49
Gefitinib	0.052 ± 0.003	–	–
Sorafenib	–	0.048 ± 0.002	–
Dox	–	–	3.62 ± 0.21

Table 4. DNA binding assay results (IC_{50}, μM) of compounds **5a** and **6g**.

DNA-active compounds	DNA/methyl green (IC_{50} μM)
5a	33.17 ± 1.7
6g	42.03 ± 2.1
Dox	31.54 ± 1.5

IC_{50} values represent the concentration (mean ± SD, $n = 3$–5 separate determinations) required for a 50% decrease in the initial absorbance of the DNA/methyl green solution.

5a and **6g** induced apoptosis in the G_0-G_1 phase by 36.93% and 38.91%, respectively, while untreated cells revealed 44.82% apoptosis. In the S phase, **5a** reported high effect (49.06%) compared to the untreated cells (36.59%), while **6g** exhibited 27.28% apoptotic effect. In G_2/M phase, compound **5a** showed 14.01% apoptotic effect whereas **6g** revealed 33.81% inhibition and control cells exhibited 18.59%. Thus, it was well established that compound **5a** arrested growth at the S phase, whereas compound **6g** produces its apoptotic activity *via* arresting cell growth at G_2/M.

Detection of apoptosis

The percentage of apoptosis induced by compounds **5a** and **6g** using HepG-2 cells was further determined using Annexin V-FITC/propidium iodide double staining flow cytometry assay[32]. As shown in Figures 5 and 6 and Table 6, compounds **5a** and **6g** induced the early apoptosis in HepG-2 cells after 24 h incubation by 12.24% and 11.02%, respectively, compared to the untreated cells (0.37%). In addition, the target compounds enhanced the late apoptotic induction by 25.13% and 19.85% compared to untreated control 0.12%. Moreover, they promoted necrosis of the cells by 7.12% and 5.41%, compared to untreated cells which showed 1.68%. Cumulatively, compounds **5a** and **6g** enhanced the total apoptosis by 37.37% and 30.87%, respectively in comparison to control cells (0.39).

Table 5. Effect of compounds **5a** and **6g** on the cell cycle distribution in HepG-2 cells.

	Cell cycle distribution (%)			
Comp. no.	G_0-G_1	S	G_2/M	Pre-G_1
5a/HepG-2	36.93	49.06	14.01	44.49
6g/HepG-2	38.91	27.28	33.81	36.28
Control	44.82	36.59	18.59	2.17

Molecular Docking study

Molecular docking has been shown to be useful tool in the field of drug discovery for explaining the interaction of small molecules with various biological targets, giving us the chance to optimise and develop better therapeutic agents[33–38]. Biological evaluation of the newly synthesised compounds revealed the outstanding potency of compound **5a** against Topo II, VEGFR2, and EGFR; that was even higher or comparable to the standard inhibitors, while compound **6g** showed moderate activity.

To inspect how far our main hypothesis in designing the target compounds was achieved in relation to the enzyme inhibitory activity, molecular docking study was utilised to investigate the potential binding mode of compounds under investigation and

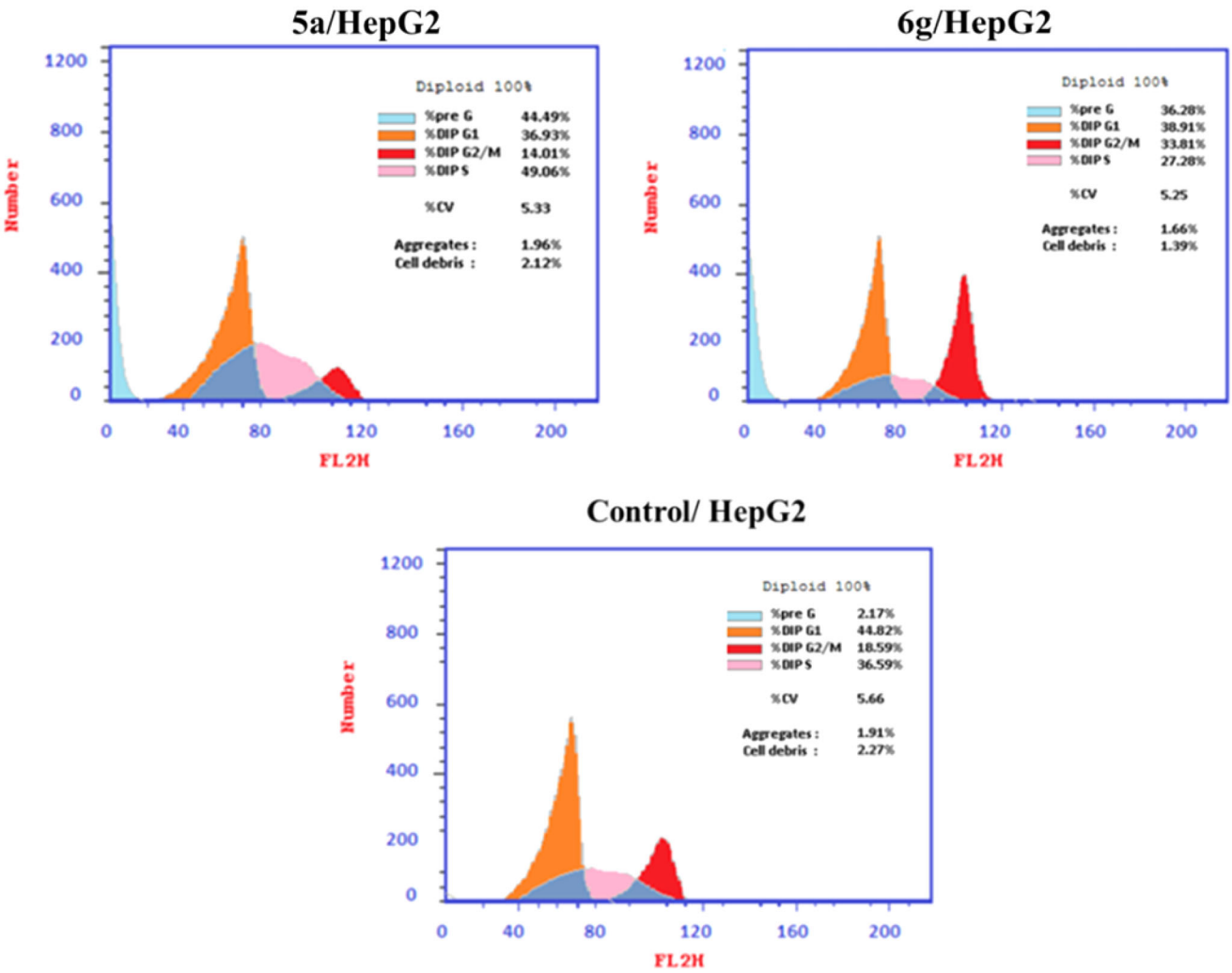

Figure 4. Flow cytometry analysis of DNA ploidy in HepG-2 cells after treatment with compounds **5a** and **6g**.

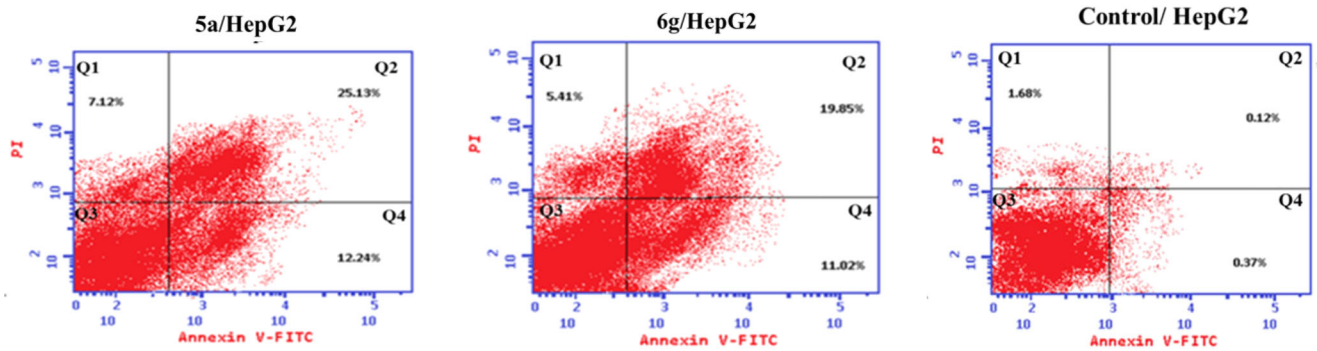

Figure 5. Effect of compounds **5a** and **6g** on the percentage of Annexin V-FITC-positive staining in HepG-2 cells. The cells were treated with DMSO as a control, **5a** and **6g** for 24 h. Q1: Necrotic cells, Q2: Late apoptosis, Q3: Live cells, Q4: early apoptosis.

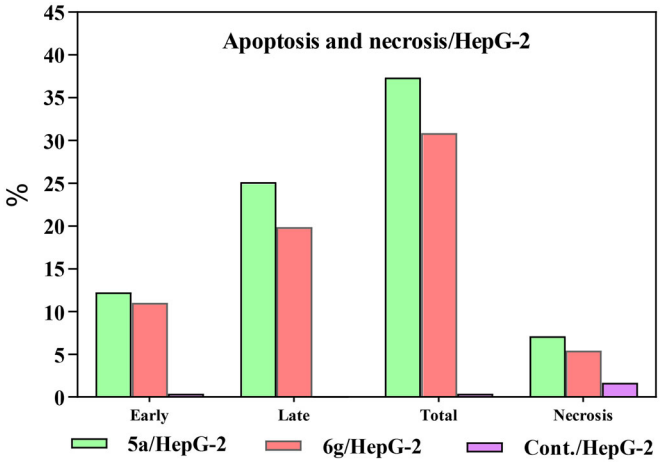

Figure 6. Early, late, total apoptosis, and necrosis induced by compounds **5a** and **6g** in HepG-2 cells compared to control.

Table 6. Apoptosis and necrosis induction analysis in HepG-2 cells after treatment with compounds **5a** and **6g**.

	Apoptosis			
Compound	Total	Early	Late	Necrosis
5a/HepG-2	37.37	12.24	25.13	7.12
6g/HepG-2	30.87	11.02	19.85	5.41
Control	0.39	0.37	0.12	1.68

Table 7. The binding energy of compound **5a** and **6g** in comparison to the co-crystallised ligand for each prospective target.

No.	Compound	Topo II	VEGFR-2	EGFR
1	**5a**	−36.4	−34.1	−28.6
2	**6g**	−33	−27.8	−22.4
3	Topo II co-crystallised ligand	−45	–	–
4	VEGFR-2 co-crystallised ligand	–	−43.9	–
5	EGFR co-crystallised ligand	–	–	−27.8

their interaction with the specified enzymes' active sites. Both of compounds **5a** and **6g** showed good binding energy in comparison to the co-crystallised ligand, still compound **5a** showed better higher affinity which agrees with the results of enzyme inhibition assay data as shown in Table 7.

Analysis of binding mode of docked compounds in Topo II enzyme

ATP active site in Topo II enzyme was selected as the binding site for the molecular docking, both of compounds **5a** and **6g** showed good fitting to catalytic site of Topo II suggesting competitive inhibition mode like that reported for this type of inhibitors[39,40]. However compound **5a** showed different binding pattern than **6g** where in case of the first, the benzimidazole ring was able to interact with the same amino acid residues interacting with adenine moiety of ATP, allowing hydrophobic interactions with Asn91, Ile125, and Phe142, also the triazole ring was in position to make extensive interaction with Ser148 and Asn150 through hydrogen bonding, mimicking ribose ring of ATP. Finally, the carbonyl and NH of carbothio(oxa)amide were able to interact through hydrogen bonding with Asn162, Asn163, Gly164, and Glu87, respectively, confirming the importance of such linker in achieving good inhibitory activity. In contrast, compound **6g** showed inverted binding mode which could explain its lower inhibitory activity in comparison to **5a** as shown in the enzyme inhibition assay. Nevertheless, the benzimidazole ring occupied the same site of triphosphate moiety; allowing the interaction with Arg162, Asn163, Gly164 through hydrogen bonding, and Gly166, Lys378 through hydrophobic interaction, still the triazole ring maintained its ability to form extensive hydrogen bonding with Ser148, Ser149, and Asn150 while the benzylidene formed hydrogen bond with Asn120 and Thr215. The interaction of compound **5a** and **6g** with ATP active site is depicted in Figures 7 and 8.

Analysis of binding mode of docked compounds in VEGFR-2 enzyme

Regarding the binding mode of compounds **5a** and **6g** in VEGFR-2, both of them showed the typical binding mode of VEGFR-2 inhibitors; where the heterocyclic ring formed hydrophobic interactions with ATP active site, also triazole rings forming hydrophobic interaction with Phe1045, Cys1043, and Val846 acting as bridge, allowing the carbothio(oxa)amide of **5a** and hydrazide of **6g** to form hydrogen bond with Asp1044 and Glu883 which is necessary to exert good inhibitory activity against this type of enzymes[41]. Interestingly, it seems that carbothio(oxa)amide linker is responsible for the better enzyme inhibition activity observed experimentally; as it formed bidentate hydrogen bond with Glu883 and give the aromatic ring of **5a** better chance to fully occupy the hydrophobic pocket of the allosteric site of VEGFR-2 interacting with Leu887, Glu883, and Gly1046 as demonstrated in Figure 9. While in case of **6g** the benzylidene moiety was able to exert hydrophobic interaction with the hydrophobic pocket but with less extent than **5a**. It is worthy to note that unlike Sorafenib, a known inhibitor of VEFFR-2, both of **5a** and **6g** were not able to interact with Cys917, an interaction that is reported to promote the inhibitory activity to nanomolar range, which might explain the promoted potency of Sorafenib over both compounds

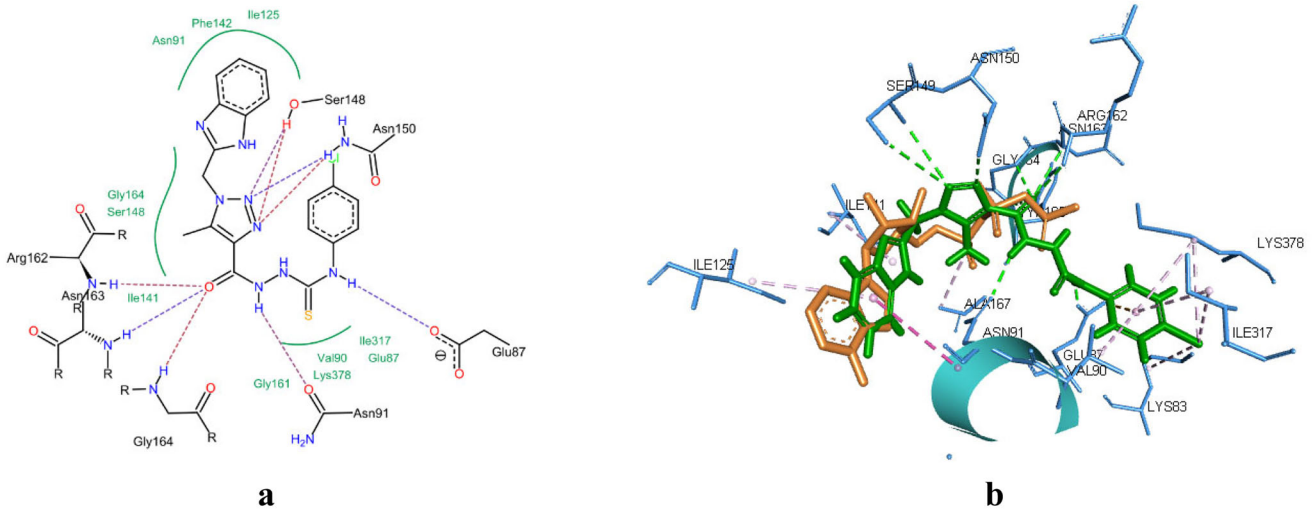

Figure 7. (a) 2D interaction of compound **5a** with Topo II active site (PDB code: 1ZXM). (b) Aligned conformation of compound **5a** (Green) with co-crystallised ligand (Salmon) inside Topo II.

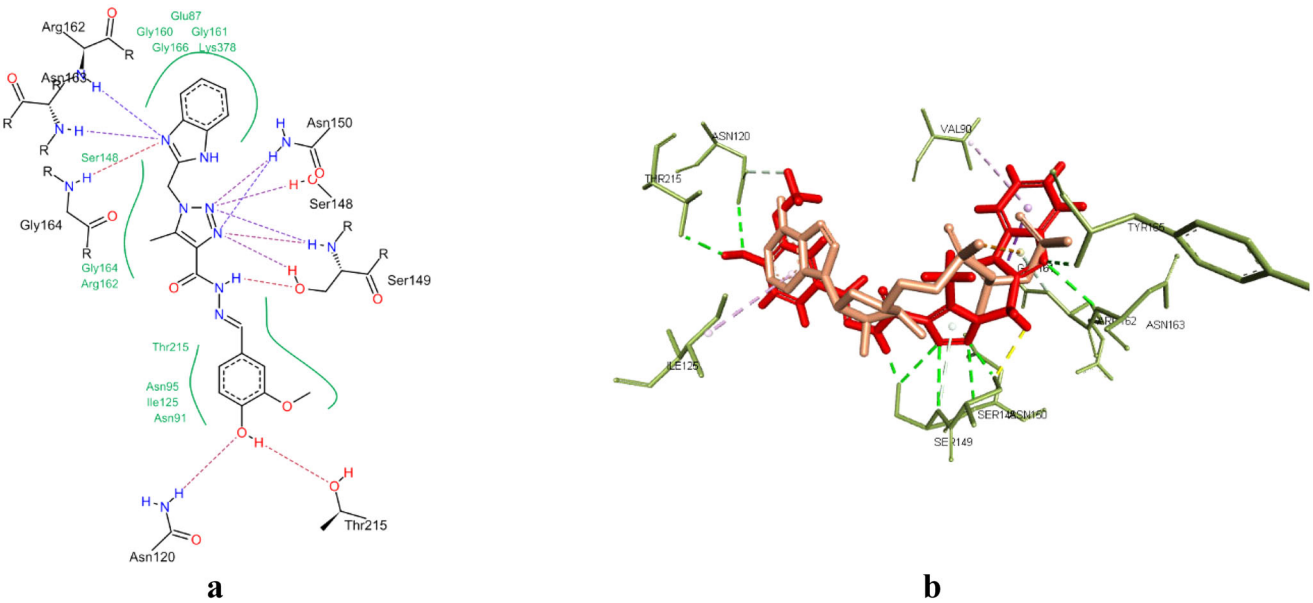

Figure 8. (a) 2D interaction of compound **6g** with Topo II active site (PDB code: 1ZXM). (b) Aligned conformation of compound **6g** (Red) with co-crystallised ligand (Salmon) inside Topo II.

in the experimental enzyme inhibition assay. The interactions of compounds **5a** and **6g** are demonstrated in Figures 9 and 10.

Analysis of binding mode of docked compounds in EGFR enzyme

Finally, the assessment of binding mode of compounds **5a** and **6g** revealed that compound **5a** is more aligned to the co-crystallised ligand than **6g** which protrude from its binding site, explaining the better enzyme inhibitory activity of **5a** over **6g**. Yet, both of them was not able to interact with Met793 residue through hydrogen bonding but **5a** interacted with it through hydrophobic interaction which was reported to be important for good docking in the enzyme[42]. This is in agree with experimental enzyme inhibition assay, where Gefitinib, an inhibitor for EGFR, showed better inhibition than compounds **5a** and **6g**. Even so, this was compensated by forming hydrogen bond with Cys797 and Phe795 for **5a** and with Asp800 and Pro794 with **6g**, allowing them to achieve comparable enzyme inhibition activity, which is shown in Figures 11 and 12.

Physicochemical properties and Lipinski's rule

Compounds **5a** and **6g** that showed the highest cytotoxicity against the tested cancer cell lines; concomitant with good safety profiles on normal cells; were further evaluated for their compliance to Lipinski's rule of five to inspect their physicochemical properties which are crucial for drug's pharmacokinetics in the human body, and; hence, predicting their putative drug-likeness (Table 8). The specified parameters were calculated with the aid of the integrated online platform pkCSM (http://structure.bio.cam.ac.uk/pkcsm)[43]. It was worthy noted that both compounds **5a** and **6g** had no violations for Lipinski's rule, whereas Dox displayed three violations, since its molecular weight exceeded 500 Daltons, it had more than five hydrogen bond donors, in addition to possessing more than ten hydrogen bond acceptors. Furthermore,

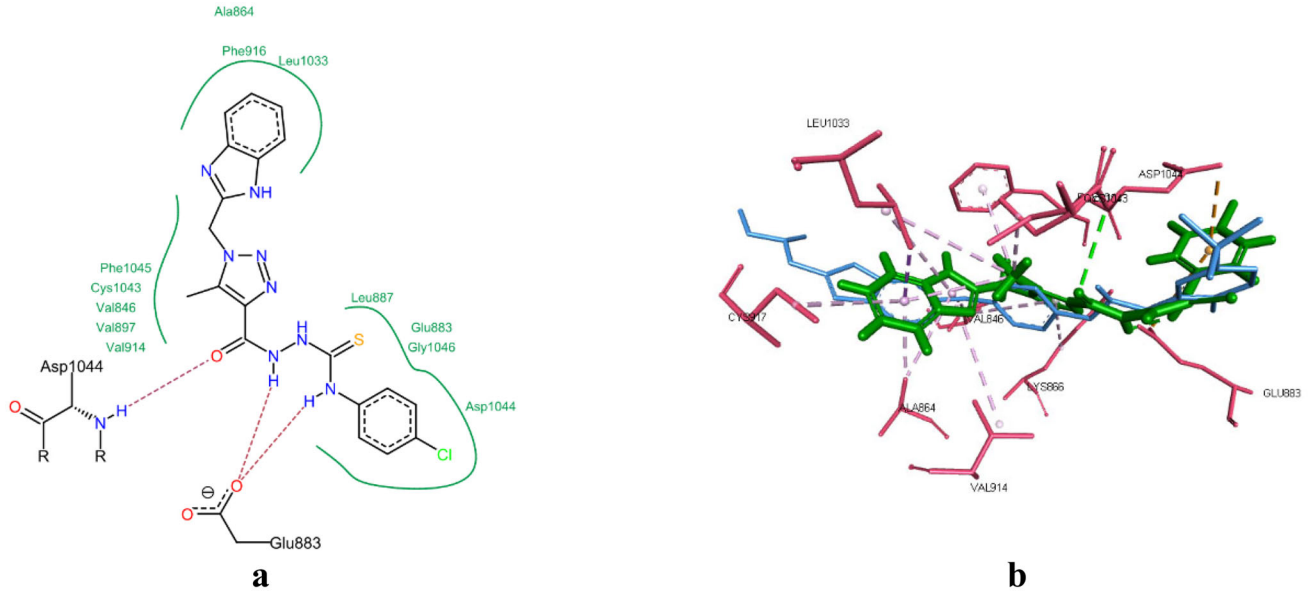

Figure 9. (a) 2D interaction of compound **5a** with VEGFR-2 active site (PDB code: 2OH4). (b) Aligned conformation of compound **5a** (Green) with co-crystallised ligand (Cyan) inside VEGFR-2.

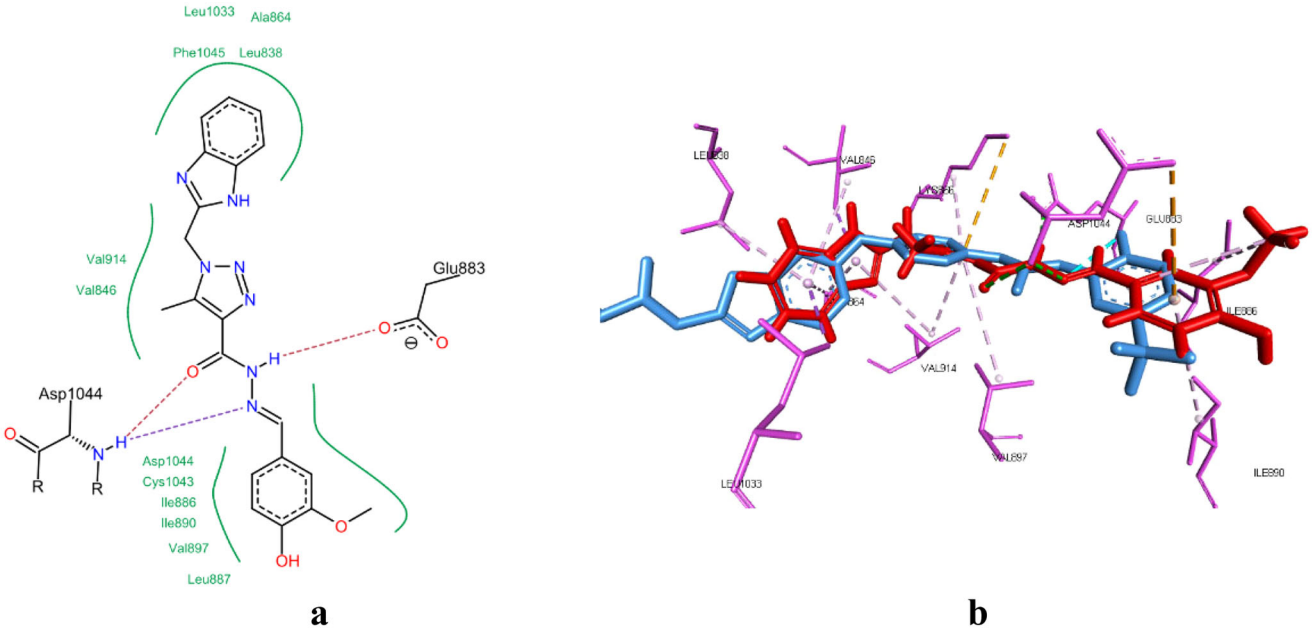

Figure 10. (a) 2D interaction of compound **6g** with VEGFR-2 active site (PDB code: 2OH4). (b) Aligned conformation of compound **6g** (Red) with co-crystallised ligand (Cyan) inside VEGFR-2.

Sorafenib violated the rule concerning lipophilicity. Moreover, the topological surface area values for both compounds **5a** and **6g** are smaller than those of either Dox, Sorafenib, or Gefitinib, thus they may serve better passive oral absorption in comparison to Dox.

Radar Plot

The bioavailability radar plot was employed to assess the dug-likeness *via* the SwissADME software[44]. Compounds **5a** and **6g** exhibited enhanced parameters concerning size and polarity over Dox (Figure 13). It was noted that degree of insaturation was slightly deviated than Dox, but better than that of Sorafenib, giving an overall good impact about their drug-likeness.

Conclusion

The main purpose of this study was to develop multi target-based benzimidazole-triazole hybrids **5a-h** and **6a-g**, aiming to promote future achievements in discovering target-specific anticancer drug candidates. The new series have been designed, prepared, and investigated as potential multi-targeting cytotoxic agents. The *in vitro* antitumor activity, EGFR, VEGFR-2 and Topo II inhibition, DNA binding assay, cell cycle analysis, and apoptotic induction have been evaluated. Among the tested hybrids, compounds **5a** ($IC_{50} \simeq 3.87–8.34\,\mu M$) and **6g** ($IC_{50} \simeq 3.34–10.92\,\mu M$) were the most potent antitumor agents against HepG-2, HCT-116, MCF-7, and HeLa cancer cells lines, with activity comparable to that of Dox ($IC_{50} \simeq 4.17–5.57\,\mu M$). In addition, they showed good safety profiles on normal cells. Also, both compounds displayed good inhibitory activity against EGFR, VEGFR-2, and Topo II. The

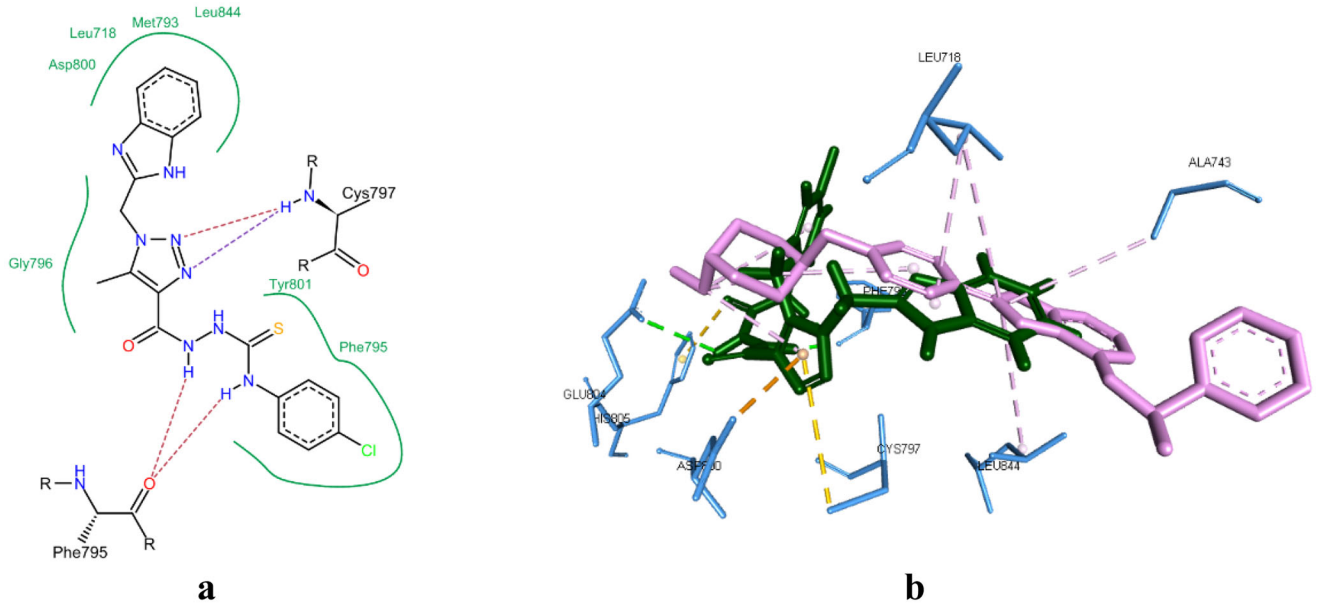

Figure 11. (a) 2D interaction of compound **5a** with EGFR active site (PDB code: 2J6M). (b) Aligned conformation of compound **5a** (Green) with co-crystallised ligand (Magenta) inside EGFR.

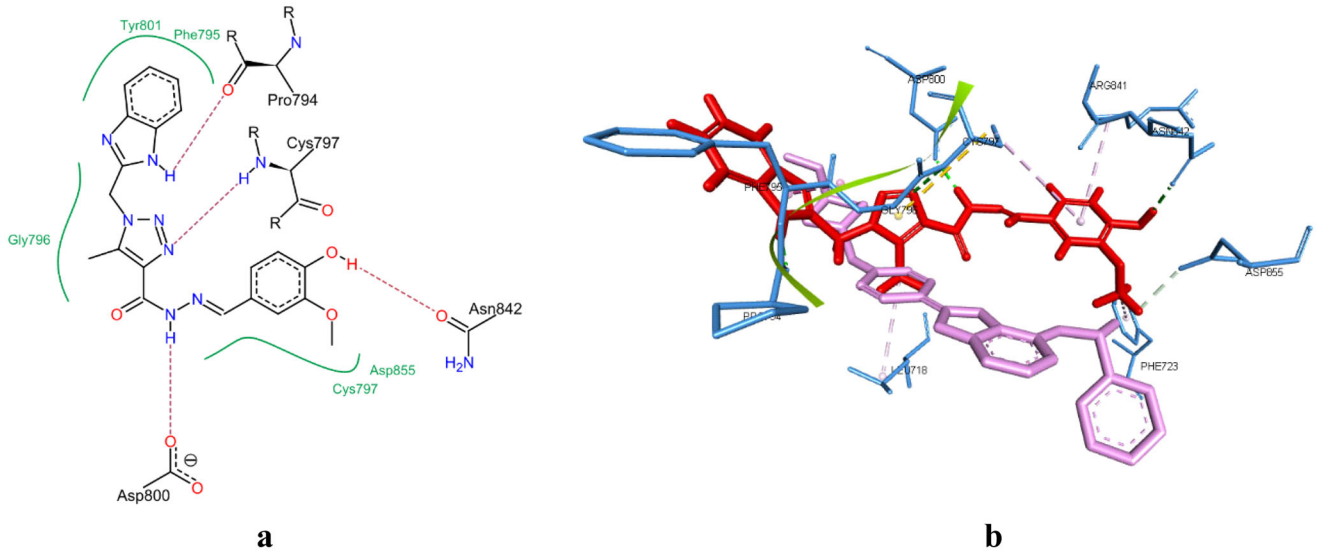

Figure 12. (a) 2D interaction of compound **6g** with EGFR active site (PDB code: 2J6M). (b) Aligned conformation of compound **6g** (Red) with co-crystallised ligand (Magenta) inside EGFR active site.

Table 8. Calculated Lipinski's rule of five for compound **5a**, **6g**, Dox, Sorafenib, and Gefitinib.

Compound	Log P	TPSA	MW	nHBA	nHBD	nRB	nVs
5a	2.7959	181.354	440.920	6	4	4	0
6g	1.9892	170.761	405.418	8	3	6	0
Dox	0.0013	222.081	543.525	12	6	5	3
Sorafenib	5.5497	185.111	464.831	4	3	5	1
Gefitinib	4.2756	184.642	446.910	7	1	8	0

Log P: octanol-water partition coefficient; TPSA: topological surface area; MW: molecular weight; nHBA: number of hydrogen bond acceptors; nHBD: number of hydrogen bond donors; nRB: number of rotatable bonds; nVs: number of violations of Lipinski's rule.

benzimidazole derivative **5a** specially exhibited good inhibitory activity against EGFR ($IC_{50} = 0.086\,\mu M$) in comparison with Gefitinib ($IC_{50} = 0.052\,\mu M$). Moreover, it exerted strong inhibitory activity on Topo II ($IC_{50} = 2.52\,\mu M$) which is better than Dox ($IC_{50} = 3.62\,\mu M$). Whereas compound **6g** exhibited moderate inhibitory activity ($IC_{50} \simeq 0.131 - 8.37\,\mu M$) on EGFR, VEGFR-2, and Topo II. The most active compound, **5a**, showed apoptosis-inducing activity of 44.49% using HepG-2 cancer cells and the cell cycle was arrested at a G1/S phase. Besides, compound **5a** exhibited nearly similar DNA intercalative activity ($IC_{50} = 33.17\,\mu M$) as Dox ($IC_{50} = 31.54\,\mu M$), where compound **6g** gave better binding than Dox with IC_{50} of $42.03\,\mu M$. The SAR

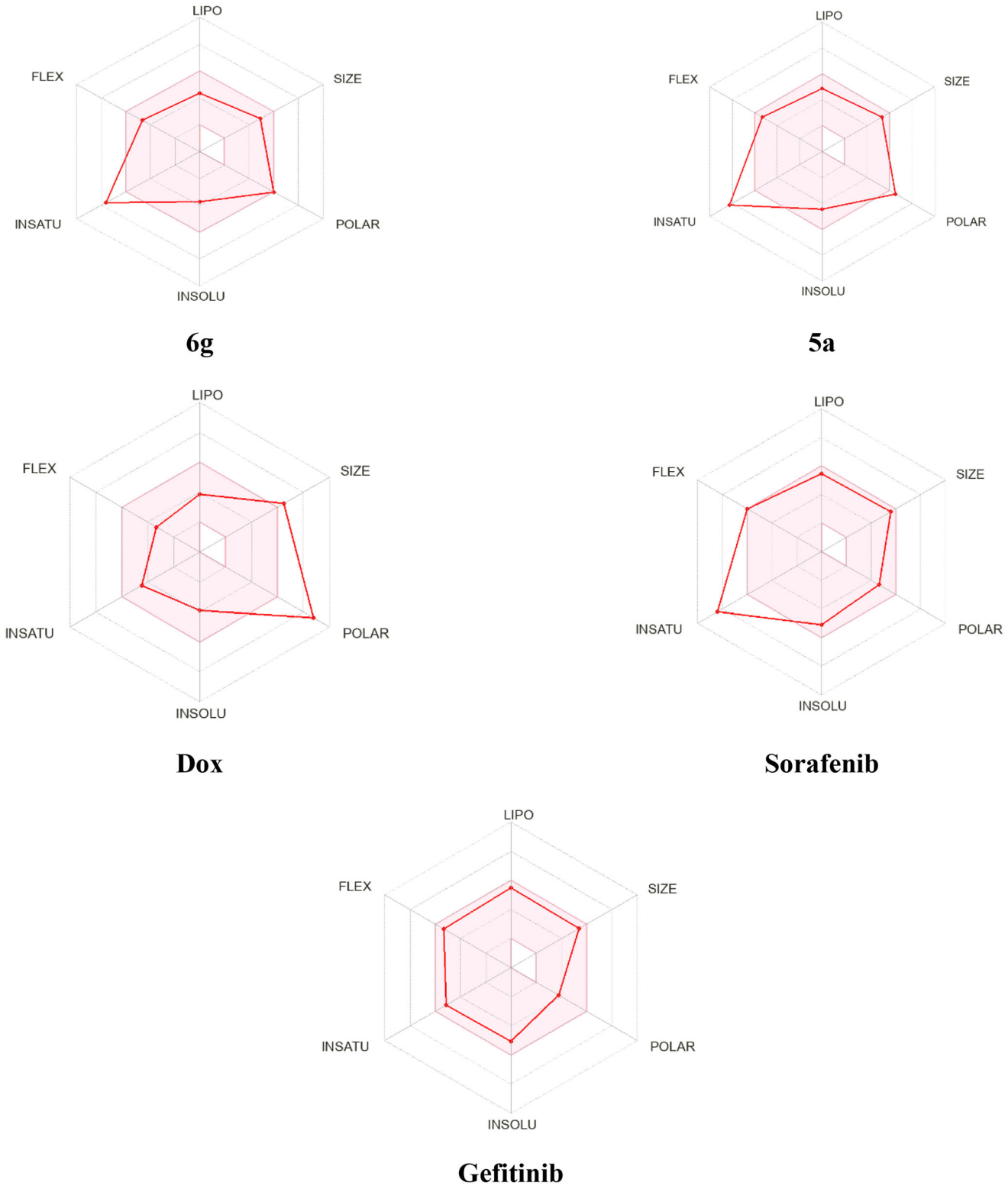

Figure 13. Bioavailability radar plot for compounds **5a**, **6g**, Dox, Sorafenib, and Gefitinib.

indicated that carbothioamide linker in series **5a-h** and the presence of electron donating groups in arylidene derivatives **6a-g** gave much contribution to the cytotoxic activity. The anti-tumor activity, as well as EGFR, VEGFR-2, and Topo II inhibitory activities were further explained using molecular modelling studies, that apparently displayed good binding with the key active sites.

Experimental part

Chemistry

All melting points (°C) were measured on Stuart melting point apparatus (SMP 30) and are uncorrected. IR spectra (KBr) were recorded on FT-IR 200 spectrophotometer (ύ cm^{-1}), Faculty of Pharmacy, Mansoura University. ^{1}H-NMR and ^{13}C-APT NMR spectra

were recorded in (DMSO-d_6) at ^{1}HNMR (400 MHz), ^{13}CNMR (100 MHz) on an NMR spectrometer (δ ppm) using TMS as an internal standard, NMR Unit, Faculty of Pharmacy, Mansoura University. Abbreviations are as follows: s, singlet; d, doublet; t, triplet; m, multiplet; br, broad. Mass spectra were carried out on direct inlet part to mass analyser in Thermo Scientific GCMS model ISQ at the Regional Centre for Mycology and Biotechnology (RCMB), Al-Azhar University, Egypt. Microanalyses were performed at Cairo University using Perkin-Elmer 240 elemental analyser for C, H, N, and S elements, and the results were within the acceptable range of the theoretical values. Compounds were detected with 254 nm UV lamp. All the chemicals and reagents used were purchased from Aldrich Chemicals Co, USA and commercial sources. Reaction times were determined using TLC on silica gel plates 60F245 E. Merk, using (EtOAc/Pet. ether; 1:1) as eluting system and the spots were visualised by UV (366–245 nm). The key precursor compound **1** and intermediate compound **2** were prepared according to the reported procedures in literature[23].

General procedure for synthesis of ethyl 1-[(1H-benzo[d]imidazol-2-yl)methyl]-5-methyl-1H-1,2,3-triazole-4-carboxylate (3)

To a stirred solution of the azide **2** (1.2 g, 7 mmol) and ethyl acetoacetate (1.0 g, 7.7 mmol) in anhydrous DMSO (15 ml), K_2CO_3 (0.38 g, 2.8 mmol) was slowly added, where the resulting suspension was stirred at rt for 48 h. The reaction mixture was then diluted with H_2O (60 ml), and the precipitated ester **3** was filtered and crystallised from pet. ether/EA mixture as pale-yellow crystals; (1.1 g, 65%). M.p. 212–214 °C. IR (ν max/cm^{-1}): 3407 (NH), 1719 (C = O). ^{1}HNMR (400 MHz, $CDCl_3$) δ 7.81–7.70 (m, 2H), 7.56–7.44 (m, 2H), 6.45 (s, 2H), 4.30 (q, J = 7.1 Hz, 2H), 2.70 (s, 3H), 1.27 (t, J = 7.1 Hz, 3H). Anal. Calcd. for $C_{14}H_{15}N_5O_2$ (285.30): C, 58.94; H, 5.30; N, 24.55. Found: C, 58.69; H, 5.42; N, 24.50%.

General procedure for synthesis of 1-[(1H-benzo[d]imidazol-2-yl)methyl]-5-methyl-1H-1,2,3-triazole-4-carbohydrazide (4)

To a solution of the ester **3** (1.00 g, 3.5 mmol) in ethanol, hydrazine hydrate (0.5 g, 10.0 mmol) was added, then the mixture was stirred at rt overnight. The precipitated solid was filtered, crystallised from ethanol to afford the target hydrazide **4** as a white solid; (0.55 g, 58%). M.p. 245–247 °C. ^{1}HNMR (400 MHz, DMSO) δ 12.67 (s, 1H), 9.67 (s, 1H), 7.55–7.65 (m, 2H), 7.19–7.20 (m, 2H), 5.88 (s, 2H), 4.45 (s, 2H), 2.57 (s, 3H). ^{13}C-APT NMR (100 MHz, DMSO) δ 160.8, 148.6, 143.2, 137.9, 137.0, 134.7, 123.4, 122.1, 119.3, 112.0, 45.9, 8.9. Anal. Calcd. for $C_{12}H_{13}N_7O$ (271.28): C, 53.13; H, 4.83; N, 36.14. Found: C, 53.10; H, 4.75; N, 36.20%.

General procedure for synthesis of carbothio(oxa)amide derivatives 5a-h

To a solution of the hydrazide **4** (0.09 g, 0.35 mmol) in THF, the appropriate iso(thio)cyanate derivative (0.3 mmol) was added, where the reaction mixture was stirred overnight at room temperature. The precipitated solid was filtered, crystallised from ethanol to afford the target derivatives **5a-h**.

2-{1-[(1h-Benzo[d]imidazol-2-yl)methyl]-5-methyl-1H-1,2,3-triazole-4-carbonyl}-N-(4-chlorophenyl) hydrazinecarbothioamide (5a). White solid; (0.083 g, 59%). M.p. 153–155 °C. IR (ν max/cm^{-1}): 3451, 3213 (NHs), 1684 (C = O). ^{1}H NMR (400 MHz, DMSO) δ 12.73 (s, 1H), 10.52 (s, 1H), 9.83 (s, 1H), 9.81 (s, 1H), 7.61–7.47 (m, 4H), 7.37 (d, J = 8.4 Hz, 2H), 7.29 (d, J = 8.4 Hz, 2H), 5.92 (s, 2H), 2.62 (s, 3H). ^{13}CNMR (100 MHz, DMSO) δ 161.6, 159.1, 148.9, 142.3, 139.3, 138.8, 136.7, 134.8, 128.9, 125.8, 123.1, 122.1, 120.5, 119.4, 112.4, 45.9, 8.9. MS m/z (%): 440.71 (M$^+$, 27.65), 442.30 (M$^+$ +2, 10.08). Anal. Calcd. for $C_{19}H_{17}ClN_8OS$ (440.91): C, 51.76; H, 3.89; N, 25.41; S, 7.27. Found: C, 51.88; H, 3.89; N, 25.45; S, 7.29%.

2-{1-[(1h-Benzo[d]imidazol-2-yl)methyl]-5-methyl-1H-1,2,3-triazole-4-carbonyl}-N-(4-chlorophenyl) hydrazinecarboxamide (5b). White solid; (0.102 g, 71%). M.p. 184–186 °C. IR (ν max/cm^{-1}): 3537, 3323, 3252 (NHs), 1694 (C = O). ^{1}HNMR (400 MHz, DMSO) δ 12.70 (s, 1H), 10.22 (s, 1H), 8.96 (s, 1H), 8.25 (s, 1H), 7.67–7.44 (m, 4H), 7.31 (d, J = 8.8 Hz, 2H), 7.26 (d, J = 8.8 Hz, 2H), 5.92 (s, 2H), 2.60 (s, 3H). ^{13}CNMR (100 MHz, DMSO) δ 161.6, 156.1, 148.6, 143.3, 139.3, 138.2, 137.4, 134.8, 128.9, 125.8, 123.1, 122.1, 120.5, 119.4, 112.0, 45.9, 8.9. MS m/z (%): 424.99 (M$^+$, 39.26), 426.30 (M$^+$+2, 11.08). Anal. Calcd. for $C_{19}H_{17}ClN_8O_2$ (424.84): C, 53.71; H, 4.03; N, 26.38. Found: C, 53.66; H, 4.23; N, 26.44%.

2-{1-[(1h-Benzo[d]imidazol-2-yl)methyl]-5-methyl-1H-1,2,3-triazole-4-carbonyl}-N-(naphthalen-1-yl)hydrazinecarboxamide (5c). White solid; (0.105 g, 79%). M.p. 233–235 °C. ^{1}HNMR (400 MHz, DMSO) δ 12.70 (s, 1H), 10.33 (s, 1H), 8.86 (s, 1H), 8.46 (s, 1H), 8.12 (d, J = 7.7 Hz, 1H), 7.94 (d, J = 7.7 Hz, 1H), 7.86–7.70 (m, 1H), 7.67 (d, J = 8.1 Hz, 1H), 7.61–7.50 (m, 4H), 7.47 (d, J = 8.1 Hz, 1H), 7.20–7.19 (m, 2H), 5.93 (s, 2H), 2.62 (s, 3H). ^{13}CNMR (100 MHz, DMSO) δ 161.5, 156.9, 148.6, 143.4, 138.3, 137.4, 134.8, 134.2, 128.8, 126.4, 126.3, 126.11, 124.00, 123.9, 123.2, 122.4, 122.3, 122.1, 121.7, 119.3, 112.1, 45.9, 8.9. MS m/z (%): 440.33 (M$^+$, 31.51). Anal. Calcd. for $C_{23}H_{20}N_8O_2$ (440.46): C, 62.72; H, 4.58; N, 25.44. Found: C, 62.66; H, 4.68; N, 25.45%.

2-{1-[(1h-Benzo[d]imidazol-2-yl)methyl]-5-methyl-1H-1,2,3-triazole-4-carbonyl}-N-phenylhydrazinecarbothioamide (5d). White solid; (0.088 g, 67%). M.p. 157–159 °C. ^{1}HNMR (400 MHz, DMSO) δ 10.79 (s, 1H), 7.63 (d, J = 7.9 Hz, 2H), 7.61–7.56 (m, 2H), 7.41–7.37 (m, 2H), 7.23 (dd, J = 7.9, 3.1 Hz, 2H), 7.05–7.01 (m, 1H), 5.99 (s, 2H), 2.68 (s, 3H). ^{13}CNMR (100 MHz, DMSO) δ 159.9, 152.7, 148.4, 139.0, 136.0, 131.5, 130.6, 129.6, 128.8, 126.4, 122.8, 122.4, 119.6, 117.5, 97.6, 46.2, 9.2. MS m/z (%): 406.42 (M$^+$, 25.20). Anal. Calcd. for $C_{19}H_{18}N_8OS$ (406.46): C, 56.14; H, 4.46; N, 27.57; S, 7.89. Found: C, 56.16; H, 4.33; N, 27.59; S, 7.95%.

2-{1-[(1h-Benzo[d]imidazol-2-yl)methyl]-5-methyl-1H-1,2,3-triazole-4-carbonyl}-N-(4-nitrophenyl) hydrazinecarboxamide (5e). Yellow solid; (0.102 g, 71%). M.p. 247–249 °C. ^{1}HNMR (400 MHz, DMSO) δ 12.71 (s, 1H), 10.33 (s, 1H), 9.62 (s, 1H), 8.57 (s, 1H), 8.19 (d, J = 9.1 Hz, 2H), 7.75 (d, J = 9.1 Hz, 2H), 7.63–7.48 (m, 2H), 7.27–7.09 (m, 2H), 5.92 (s, 2H), 2.60 (s, 3H). ^{13}CNMR (100 MHz, DMSO) δ 161.8, 157.5, 153.8, 148.6, 147.0, 143.5, 141.5, 138.4, 137.3, 134.8, 125.5, 123.1, 122.1, 119.4, 112.1, 45.9, 8.9. MS m/z (%): 435.54 (M$^+$, 22.26). Anal. Calcd. for $C_{19}H_{17}N_9O_4$ (435.40): C, 52.41; H, 3.94; N, 28.95. Found: C, 52.36; H, 3.98; N, 28.88%.

2-{1-[(1h-Benzo[d]imidazol-2-yl)methyl]-5-methyl-1H-1,2,3-triazole-4-carbonyl}-N-(p-tolyl)hydrazinecarbothioamide (5f). White solid; (0.090 g, 64%). M.p. 257–259 °C. ^{1}H NMR (400 MHz, DMSO) δ 12.72 (s, 1H), 10.66 (s, 1H), 7.72–7.52 (m, 2H), 7.51 (d, J = 7.3 Hz, 2H), 7.31–7.23 (m, 2H), 7.18 (d, J = 7.3 Hz, 2H), 5.97 (s, 2H), 2.67 (s, 3H), 2.28 (s, 3H). ^{13}C NMR (100 MHz, DMSO) δ 160.0, 152.6, 148.4, 136.6, 136.0, 131.5, 131.3, 129.9, 123.2, 123.1 122.1 119.4, 119.3, 117.5, 112.1, 46.3, 20.8, 9.1. MS m/z (%): 420.31 (M$^+$, 33.56). Anal.

Calcd. for $C_{20}H_{20}N_8OS$ (420.49): C, 57.13; H, 4.79; N, 26.65; S, 7.63. Found: C, 57.26; H, 4.79; N, 26.69; S, 7.60%.

2-{1-[(1h-Benzo[d]imidazol-2-yl)methyl]-5-methyl-1H-1,2,3-triazole-4-carbonyl}-N-(4-methoxyphenyl)hydrazinecarbothioamide (5g). White solid; (0.079 g, 56%). M.p. 235–237 °C. ^{1}HNMR (400 MHz, DMSO) δ 12.71 (s, 1H), 10.55 (s, 1H), 7.64–7.54 (m, 2H), 7.52 (d, $J = 7.9$ Hz, 2H), 7.26–7.17 (m, 2H), 6.97 (d, $J = 7.9$ Hz, 2H), 5.97 (s, 2H), 3.75 (s, 3H), 2.66 (s, 3H). ^{13}CNMR (101 MHz, DMSO) δ 162.9, 160.1, 154.9, 152.5, 148.4, 135.9, 132.3, 131.5, 123.2, 122.2, 119.9, 119.3, 119.0, 114.8, 112.1, 55.7, 46.2, 9.1. MS m/z (%): 436.02 (M^+, 20.15). Anal. Calcd. for $C_{20}H_{20}N_8O_2S$ (436.49): C, 55.03; H, 4.62; N, 25.67; S, 7.35. Found: C, 55.03; H, 4.60; N, 25.69; S, 7.25%.

2-{1-[(1h-Benzo[d]imidazol-2-yl)methyl]-5-methyl-1H-1,2,3-triazole-4-carbonyl}-N-phenylhydrazinecarboxamide (5h). White solid; (0.085 g, 66%). M.p. 182–184 °C. ^{1}HNMR (400 MHz, DMSO) δ 12.69 (s, 1H), 10.19 (s, 1H), 8.79 (s, 1H), 8.15 (s, 1H), 7.61 (d, $J = 7.0$ Hz, 1H), 7.52 (d, $J = 7.0$ Hz, 1H), 7.50–7.46 (m, 2H), 7.33–7.14 (m, 4H), 7.01–6.92 (m, 1H), 5.92 (s, 2H), 2.60 (s, 3H). ^{13}CNMR (100 MHz, DMSO) δ 161.5, 155.8, 148.6, 143.3, 140.2, 138.2, 137.4, 134.8, 129.1, 123.1, 122.3, 122.1, 119.4, 118.9, 112.0, 45.9, 8.9. MS m/z (%): 390.35 (M^+, 29.66). Anal. Calcd. for $C_{19}H_{18}N_8O_2$ (390.40): C, 58.45; H, 4.65; N, 28.70. Found: C, 58.26; H, 4.80; N, 28.65%.

General procedure for synthesis of benzylidene derivatives 6a-g

To a solution of hydrazide **4** (0.09 g, 0.35 mmol) in ethanol, containing catalytic drops of glacial acetic acid, the appropriate aldehyde (0.3 mmol) was added. The mixture was refluxed overnight. Then, the reaction mixture was cooled to rt. The precipitated solid was filtered, and crystallised from ethanol to afford pure derivatives **6a-g**.

(E)-1-[(1H-Benzo[d]imidazol-2-yl)methyl]-N′-(4-chlorobenzylidene)-5-methyl-1H-1,2,3-triazole-4-carbohydrazide (6a). White solid; (0.085 g, 61%). M.p. 280–282 °C. ^{1}HNMR (400 MHz, DMSO) δ 12.70 (s, 1H), 12.18 (s, 1H), 8.57 (s, 1H), 7.73 (d, $J = 8.1$ Hz, 2H), 7.67–7.48 (m, 4H), 7.31 (d, $J = 8.1$ Hz, 2H), 5.94 (s, 2H), 2.64 (s, 3H). ^{13}CNMR (100 MHz, DMSO) δ 157.9, 148.5, 147.1, 138.9, 137.6, 134.9, 133.9, 129.4, 129.3, 129.2, 129.1, 123.1, 122.1, 119.4, 112.1, 46.0, 9.0. MS m/z (%): 393.41 (M^+, 30.25), 395.5 (M^++2, 11.08). Anal. Calcd. for $C_{19}H_{16}ClN_7O$ (393.83): C, 57.94; H, 4.09; N, 24.90. Found: C, 57.84; H, 4.12; N, 24.88%.

(E)-1-[(1H-Benzo[d]imidazol-2-yl)methyl]-N′-benzylidene-5-methyl-1H-1,2,3-triazole-4-carbohydrazide (6b). White solid; (0.072 g, 65%). M.p. 185–187 °C. IR (ν max/cm^{-1}): 3300, 3221 (NHs), 1669 (C = O). ^{1}H NMR (400 MHz, DMSO) δ 12.69 (s, 1H), 12.08 (s, 1H), 8.58 (s, 1H), 7.71 (d, $J = 6.3$ Hz, 2H), 7.65–7.38 (m, 5H), 7.29–7.07 (m, 2H), 5.94 (s, 2H), 2.65 (s, 3H). ^{13}CNMR (100 MHz, DMSO) δ 157.8, 148.5, 148.4, 138.8, 137.7, 135.1, 134.9, 130.5, 130.4, 129.3, 129.3, 129.2, 127.6, 127.5, 127.5, 46.0, 9.0. MS m/z (%): 359.01 (M^+, 25.33). Anal. Calcd. for $C_{19}H_{17}N_7O$ (359.38): C, 63.50; H, 4.77; N, 27.28. Found: C, 63.56; H, 4.78; N, 27.08%.

(E)-1-[(1H-Benzo[d]imidazol-2-yl)methyl]-N′-(3-bromobenzylidene)-5-methyl-1H-1,2,3-triazole-4-carbohydrazide (6c). White solid; (0.089 g, 64%). M.p. 152–154 °C. ^{1}HNMR (400 MHz, DMSO) δ 12.79 (s, 1H), 12.24 (s, 1H), 8.55 (s, 1H), 7.91 (s, 1H), 7.67 (d, $J = 6.7$ Hz, 2H), 7.61–7.51 (m, 2H), 7.49–7.39 (m, 1H), 7.33–7.12 (m, 2H), 5.95 (s, 2H), 2.65 (s, 3H). ^{13}CNMR (100 MHz, DMSO) δ 157.9, 148.5, 146.6, 138.9, 138.9, 137.6, 137.5, 137.4, 133.0, 133.0, 131.6, 131.5, 129.5, 129.4, 126.8, 126.7, 122.6, 46.0, 9.0. MS m/z (%): 438.34 (M^+, 36.21), 440.14 (M^++2, 30.91). Anal. Calcd. for $C_{19}H_{16}BrN_7O$ (438.28): C, 52.07; H, 3.68; N, 22.37. Found: C, 52.12; H, 3.55; N, 22.27%.

(E)-1-[(1H-Benzo[d]imidazol-2-yl)methyl]-5-methyl-N′-(3-nitrobenzylidene)-1H-1,2,3-triazole-4-carbohydrazide (6d). Yellow solid; (0.076 g, 58%). M.p. 163–165 °C. ^{1}HNMR (400 MHz, DMSO) δ 12.70 (s, 1H), 12.37 (s, 1H), 8.69 (s, 1H), 8.53 (s, 1H), 8.28 (d, $J = 7.6$ Hz, 1H), 8.12 (d, $J = 7.6$ Hz, 1H), 7.87–7.72 (m, 1H), 7.72–7.44 (m, 2H), 7.33–7.12 (m, 2H), 5.95 (s, 2H), 2.66 (s, 3H). ^{13}CNMR (100 MHz, DMSO) δ 158.0, 148.7, 146.0, 139.1, 139.0, 137.6, 137.5, 136.9, 136.8, 133.9, 131.0, 131.0, 124.7, 124.7, 122.7, 121.3, 121.2, 46.0, 9.1. MS m/z (%): 404.29 (M^+, 39.55). Anal. Calcd. for $C_{19}H_{16}N_8O_3$ (404.38): C, 56.43; H, 3.99; N, 27.71. Found: C, 56.38; H, 3.92; N, 27.75%.

(E)-1-[(1H-Benzo[d]imidazol-2-yl)methyl]-N′-(3,4-dimethoxybenzylidene)-5-methyl-1H-1,2,3-triazole-4-carbohydrazide (6e). White solid; (0.093 g, 71%). M.p. 270–272 °C. ^{1}HNMR (400 MHz, DMSO) δ 12.69 (s, 1H), 11.96 (s, 1H), 8.49 (s, 1H), 7.63–7.47 (m, 2H), 7.39 (s,1H), 7.34–7.22 (m, 2H), 7.17 (d, $J = 8.2$ Hz, 1H), 7.04 (d, $J = 8.2$ Hz, 1H), 5.94 (s, 2H), 3.84 (s, 3H), 3.82 (s, 3H), 2.64 (s, 3H). ^{13}CNMR (100 MHz, DMSO) δ 157.7, 151.2, 149.5, 148.6, 148.5, 139.1, 138.6, 137.8, 137.7, 127.6, 127.5, 122.4, 122.3, 112.0, 111.9, 108.7, 108.6, 56.1, 55.9, 46.0, 9.1. MS m/z (%): 419.02 (M^+, 21.56). MS m/z (%):419.64 (M^+, 74.96). Anal. Calcd. for $C_{21}H_{21}N_7O_3$ (419.44): C, 60.13; H, 5.05; N, 23.38. Found: C, 60.11; H, 5.15; N, 23.32%.

(E)-1-[(1H-Benzo[d]imidazol-2-yl)methyl]-N′-[4-(dimethylamino)benzylidene]-5-methyl-1H-1,2,3-triazole-4-carbohydrazide (6f). White solid; (0.082 g, 60%). M.p. 268–270 °C. ^{1}HNMR (400 MHz, DMSO) δ 12.68 (s, 1H), 11.74 (s, 1H), 8.41 (s, 1H), 7.69–7.60 (m, 2H), 7.52 (d, $J = 8.7$ Hz, 2H), 7.35–7.12 (m, 2H), 6.77 (d, $J = 8.7$ Hz, 2H), 5.93 (s, 2H), 2.99 (s, 6H), 2.63 (s, 3H). ^{13}CNMR (101 MHz, DMSO) δ 157.4, 151.9, 149.2, 148.6, 138.3, 138.0, 128.9, 128.8, 123.1, 122.2, 122.1, 119.4, 112.6, 112.3, 112.1, 46.1, 40.4, 9.0. MS m/z (%): 402.41 (M^+, 28.36). Anal. Calcd. for $C_{21}H_{22}N_8O$ (402.45): C, 62.67; H, 5.51; N, 27.84. Found: C, 62.54; H, 5.50; N, 27.89%.

(E)-1-[(1H-Benzo[d]imidazol-2-yl)methyl]-N′-(4-hydroxy-3-methoxybenzylidene)-5-methyl-1H-1,2,3-triazole-4-carbohydrazide (6g). White solid; (0.091 g, 75%). M.p. 228–230 °C. IR (ν max/cm^{-1}): 3427 (OH), 3325 (NH), 1659 (C = O). ^{1}HNMR (400 MHz, DMSO) δ 12.70 (s, 1H), 11.88 (s, 1H), 9.54 (s, 1H), 8.44 (s, 1H), 7.63–7.49 (m, 2H), 7.30 (s, 1H), 7.26–7.14 (m, 2H), 7.06 (d, $J = 8.3$ Hz, 1H), 6.85 (d, $J = 8.3$ Hz, 1H), 5.93 (s, 2H), 3.85 (s, 3H), 2.64 (s, 3H). ^{13}CNMR (100 MHz, DMSO) δ 158.7, 151.2, 149.5, 148.6, 147.5, 139.1, 138.6, 137.8, 137.7, 127.6, 126.5, 122.4, 122.3, 112.0, 111.9, 108.7, 108.6, 55.7, 46.0, 9.1. MS m/z (%): 405.48 (M^+, 50.06). Anal. Calcd. for $C_{20}H_{19}N_7O_3$ (405.41): C, 59.25; H, 4.72; N, 24.18. Found: C, 59.30; H, 4.62; N, 24.09%.

Biological evaluation

In vitro cytotoxic study against HepG-2, HCT-116, MCF-7, and HeLa cell lines

The MTT assay was performed to evaluate the *in vitro* antitumor activity of the newly synthesised compounds according to the reported method[3,45,46].

In vitro cytotoxic activity of the most active compounds (5a, 6g) against WI-38 cell line

The cytotoxicity of compounds **5a** and **6g** was estimated according to the reported procedure[47].

In vitro enzyme inhibitory assays (against EGFR, VEGFR-2, and Topo II)

Enzyme inhibitory assays for the most active compounds **5a** and **6g** were carried out as described in the previous reports in the literature[48].

DNA/methyl green colorimetric method for DNA binding assay

DNA binding assay was carried out according to the reported method[29].

Flow cytometry analysis of the cell cycle distribution

Cell cycle analysis was performed using the HepG-2 cell lines stained with propidium iodide (PI) and FACSCalibur flow cytometer as mentioned in previous reports[30,31].

Analysis of cellular apoptosis

Apoptosis induction was performed using the HepG-2 cell lines and well-established Annexin 5-FITC/PI detection kit similar to the reported procedures[30,31].

Molecular docking study

Molecular docking of compounds **5a** and **6g** was done by preparing 3D structure of these compounds and the PDB of the selected targets, Top II (1ZXM) and VEGFR-2 (2OH4) and EGFR (2J6M) as previously reported[49]. Molecular docking was done using Leadit software[50,51] and the active site was set as sphere with radius 6.5 Å around the co-crystallised ligand. The software was considered valid by redocking the co-crystallised ligand and the RMSD were shown to be no more than 1.5 Å (Figures S1 and S2). The 3D structure of the compounds was selected as a library and was docked to the active site. Finally, the docked poses were inspected using Discovery studio visualiser to study their interaction with the binding site[52].

Physicochemical properties and Lipinski's rule

The physicochemical parameters were calculated for compounds **5a**, **6g**, Dox, Sorafenib, and Gefitinib using the free online website of pkCSM (http://structure.bio.cam.ac.uk/pkcsm)[43].

Radar plot

SwissADME software was employed to investigate the dug-likeness of compounds **5a** and **6g** in comparison with the reference drugs Dox, Sorafenib, and Gefitinib *via* the bioavailability radar plot[53].

Acknowledgements

This study did not receive any specific grant from funding agencies in the public, commercial, or not-for-profit sectors.

Disclosure statement

No potential conflict of interest was reported by the author(s).

Funding

The author(s) reported there is no funding associated with the work featured in this article.

Appendix A. Supplementary data

Supplementary data related to this manuscript are found in a separate file.

ORCID

Amany S. Mostafa http://orcid.org/0000-0003-1909-1072

References

1. Goud NS, Kumar P, Bharath RD. Recent developments of target-based benzimidazole derivatives as potential anticancer agents. Mini Rev Med Chem. 2020;20(17):1754–1766.
2. Mostafa AS, Gomaa RM, Elmorsy MA. Design and synthesis of 2-phenyl benzimidazole derivatives as VEGFR-2 inhibitors with anti-breast cancer activity. Chem Biol Drug Des. 2019; 93(4):454–463.
3. Hamdi A, El-Shafey HW, Othman DI, El-Azab AS, AlSaif NA, Alaa A-M. Design, synthesis, antitumor, and VEGFR-2 inhibition activities of novel 4-anilino-2-vinyl-quinazolines: molecular modeling studies. Bioorg Chem. 2022;122:105710.
4. Singh H, Kinarivala N, Sharma S. Multi-targeting anticancer agents: rational approaches, synthetic routes and structure activity relationship. Anticancer Agents Med Chem. 2019; 19(7):842–874.
5. Ibrahim HA, Refaat HM. Versatile mechanisms of 2-substituted benzimidazoles in targeted cancer therapy. Future J Pharm Sci. 2020;6(1):1–20.
6. Li Y, Tan C, Gao C, Zhang C, Luan X, Chen X, Liu H, Chen Y, Jiang Y. Discovery of benzimidazole derivatives as novel multi-target EGFR, VEGFR-2 and PDGFR kinase inhibitors. Bioorg Med Chem. 2011;19(15):4529–4535.
7. Cheson BD, Leoni L. Bendamustine: mechanism of action and clinical data. Clin Adv Hematol Oncol. 2011;9(8 Suppl 19):1–11.
8. Hasinoff BB, Wu X, Nitiss JL, Kanagasabai R, Yalowich JC. The anticancer multi-kinase inhibitor dovitinib also targets topoisomerase I and topoisomerase II. Biochem Pharmacol. 2012; 84(12):1617–1626.
9. Ali AM, Tawfik SS, Mostafa AS, Massoud MAM. Benzimidazole-based protein kinase inhibitors: current perspectives in targeted cancer therapy. Chem Biol Drug Des. 2022;100(5):656–673.
10. Musolino A, Campone M, Neven P, Denduluri N, Barrios CH, Cortes J, Blackwell K, Soliman H, Kahan Z, Bonnefoi H, et al. Phase II, randomized, placebo-controlled study of dovitinib in combination with fulvestrant in postmenopausal patients with HR+, HER2− breast cancer that had progressed during or after prior endocrine therapy. Breast Cancer Res. 2017; 19(1):1–14.
11. Nadhan R, Srinivas P, Pillai MR. RTKs in pathobiology of head and neck cancers. Adv Cancer Res. 2020;147:319–373.

12. Woei-A-Jin FJSH, Weijl NI, Burgmans MC, Fariña Sarasqueta A, van Wezel JT, Wasser MNJM, Coenraad MJ, Burggraaf J, Osanto S. Neoadjuvant treatment with angiogenesis-inhibitor dovitinib prior to local therapy in hepatocellular carcinoma: a phase II study. Oncologist. 2021;26(10):854–864.
13. Liu W-Q, Megale V, Borriello L, Leforban B, Montès M, Goldwaser E, Gresh N, Piquemal J-P, Hadj-Slimane R, Hermine O, et al. Synthesis and structure–activity relationship of non-peptidic antagonists of neuropilin-1 receptor. Bioorg Med Chem Lett. 2014;24(17):4254–4259.
14. McBride CM, Renhowe PA, Heise C, Jansen JM, Lapointe G, Ma S, Piñeda R, Vora J, Wiesmann M, Shafer CM, et al. Design and structure–activity relationship of 3-benzimidazol-2-yl-1H-indazoles as inhibitors of receptor tyrosine kinases. Bioorg Med Chem Lett. 2006;16(13):3595–3599.
15. Pinar A, Yurdakul P, Yildiz I, Temiz-Arpaci O, Acan NL, Aki-Sener E, Yalcin I. Some fused heterocyclic compounds as eukaryotic topoisomerase II inhibitors. Biochem Biophys Res Commun. 2004;317(2):670–674.
16. Nawareg NA, Mostafa AS, El-Messery SM, Nasr MN. New benzimidazole based hybrids: synthesis, molecular modeling study and anticancer evaluation as TopoII inhibitors. Bioorg Chem. 2022; 127:106038.
17. Xu Z, Zhao S-J, Liu Y. 1, 2, 3-Triazole-containing hybrids as potential anticancer agents: current developments, action mechanisms and structure-activity relationships. Eur J Med Chem. 2019;183:111700.
18. Alam MM. 1, 2, 3-Triazole hybrids as anticancer agents: a review. Arch Pharm. 2022;355(1):2100158.
19. El-Sayed WA, Alminderej FM, Mounier MM, Nossier ES, Saleh SM, Kassem AF. Novel 1, 2, 3-triazole-coumarin hybrid glycosides and their tetrazolyl analogues: design, anticancer evaluation and molecular docking targeting EGFR, VEGFR-2 and CDK-2. Molecules. 2022;27(7):2047.
20. Wang D-P, Liu K-L, Li X-Y, Lu G-Q, Xue W-H, Qian X-H, Mohamed O K, Meng F-H. Design, synthesis, and *in vitro* and *in vivo* anti-angiogenesis study of a novel vascular endothelial growth factor receptor-2 (VEGFR-2) inhibitor based on 1, 2, 3-triazole scaffold. Eur J Med Chem. 2021;211: 113083.
21. Abdel-Hafez GA, Mohamed A-MI, Youssef AF, Simons C, Aboraia AS. Synthesis, computational study and biological evaluation of 9-acridinyl and 1-coumarinyl-1, 2, 3-triazole-4-yl derivatives as topoisomerase II inhibitors. J Enzyme Inhib Med Chem. 2022;37(1):502–513.
22. Bistrović A, Krstulović L, Harej A, Grbčić P, Sedić M, Koštrun S, Pavelić SK, Bajić M, Raić-Malić S. Design, synthesis and biological evaluation of novel benzimidazole amidines as potent multi-target inhibitors for the treatment of non-small cell lung cancer. Eur J Med Chem. 2018;143:1616–1634.
23. Sahay II, Ghalsasi PS. Synthesis of new 1, 2, 3-triazole linked benzimidazole molecules as anti-proliferative agents. Synth Commun. 2017;47(8):825–834.
24. Cai M, Hu J, Tian J-L, Yan H, Zheng C-G, Hu W-L. Novel hybrids from N-hydroxyarylamide and indole ring through click chemistry as histone deacetylase inhibitors with potent antitumor activities. Chin Chem Lett. 2015;26(6):675–680.
25. Nafie MS, Boraei AT. Exploration of novel VEGFR2 tyrosine kinase inhibitors via design and synthesis of new alkylated indolyl-triazole Schiff bases for targeting breast cancer. Bioorg Chem. 2022;122:105708.
26. Al-Hussain SA, Farghaly TA, Zaki ME, Abdulwahab HG, Al-Qurashi NT, Muhammad ZA. Discovery of novel indolyl-1, 2, 4-triazole hybrids as potent vascular endothelial growth factor receptor-2 (VEGFR-2) inhibitors with potential anti-renal cancer activity. Bioorg Chem. 2020;105:104330.
27. Wang Z-J, Yang H-H, Tian L, Zhao W-G. Design, synthesis, and fungicidal activities of novel 5-methyl-1H-1, 2, 3-trizole-4-carboxyl amide analogues. Med Chem. 2016;12(3):290–295.
28. Theocharis A, Alexandrou N, Terzis A. Generation and dienophilic properties of 1-benzyl-1H-1, 2, 3-triazolo [4, 5-d] pyridazine-4, 7-dione. J Heterocycl Chem. 1990;27(6):1741–1744.
29. Burres NS, Frigo A, Rasmussen RR, McAlpine JB. A colorimetric microassay for the detection of agents that interact with DNA. J Nat Prod. 1992;55(11):1582–1587.
30. Tolba MF, Esmat A, Al-Abd AM, Azab SS, Khalifa AE, Mosli HA, Abdel-Rahman SZ, Abdel-Naim AB. Caffeic acid phenethyl ester synergistically enhances docetaxel and paclitaxel cytotoxicity in prostate cancer cells. IUBMB Life. 2013; 65(8):716–729.
31. Mosmann T. Rapid colorimetric assay for cellular growth and survival: application to proliferation and cytotoxicity assays. J Immunol Methods. 1983;65(1–2):55–63.
32. Kumar R, Saneja A, Panda AK. An annexin V-FITC—propidium iodide-based method for detecting apoptosis in a non-small cell lung cancer cell line. Lung Cancer. 2021;2279: 213–223.
33. Selim NM, Elgazar AA, Abdel-Hamid NM, El-Magd MRA, Yasri A, Hefnawy HME, Sobeh M. Chrysophanol, physcion, hesperidin and curcumin modulate the gene expression of pro-inflammatory mediators induced by LPS in HepG2: in silico and molecular studies. Antioxidants. 2019;8(9):371.
34. Elsbaey M, Ibrahim MAA, Bar FA, Elgazar AA. Chemical constituents from coconut waste and their in silico evaluation as potential antiviral agents against SARS-CoV-2. S Afr J Bot. 2021;141:278–289.
35. Elgazar AA, Selim NM, Abdel-Hamid NM, El-Magd MA, El Hefnawy HM. Isolates from *Alpinia officinarum* Hance attenuate LPS-induced inflammation in HepG2: evidence from in silico and in vitro studies. Phytother Res. 2018;32(7): 1273–1288.
36. Elgazar AA, Knany HR, Ali MS. Insights on the molecular mechanism of anti-inflammatory effect of formula from Islamic traditional medicine: an in-silico study. J Tradit Complement Med. 2019;9(4):353–363.
37. Badria FA, Elgazar AA. Chapter 37 – revealing the molecular mechanism of *Olea europaea* L. in treatment of cataract. In: Preedy VR, Watson RR, editors. Olives and olive oil in health and disease prevention. 2nd ed. San Diego: Academic Press; 2021. p. 445–456.
38. Othman DI, Hamdi A, Abdel-Aziz MM, Elfeky SM. Novel 2-arylthiazolidin-4-one-thiazole hybrids with potent activity against *Mycobacterium tuberculosis*. Bioorg Chem. 2022;124: 105809.
39. Yao B-L, Mai Y-W, Chen S-B, Xie H-T, Yao P-F, Ou T-M, Tan J-H, Wang H-G, Li D, Huang S-L, et al. Design, synthesis and biological evaluation of novel 7-alkylamino substituted benzo[a]-phenazin derivatives as dual topoisomerase I/II inhibitors. Eur J Med Chem. 2015;92:540–553.
40. Hu C-X, Zuo Z-L, Xiong B, Ma J-G, Geng M-Y, Lin L-P, Jiang H-L, Ding J. Salvicine functions as novel Topoisomerase II poison by binding to ATP pocket. Mol Pharmacol. 2006; 70(5):1593–1601.
41. Hasegawa M, Nishigaki N, Washio Y, Kano K, Harris PA, Sato H, Mori I, West RI, Shibahara M, Toyoda H, et al. Discovery of novel benzimidazoles as potent inhibitors of TIE-2 and

VEGFR-2 tyrosine kinase receptors. J Med Chem. 2007;50(18): 4453–4470.
42. Verma N, Rai AK, Kaushik V, Brünnert D, Chahar KR, Pandey J, Goyal P. Identification of gefitinib off-targets using a structure-based systems biology approach; their validation with reverse docking and retrospective data mining. Sci Rep. 2016;6(1):1–12.
43. Pires DE, Blundell TL, Ascher DB. pkCSM: predicting small-molecule pharmacokinetic and toxicity properties using graph-based signatures. J Med Chem. 2015;58(9):4066–4072.
44. Daina A, Michielin O, Zoete V. SwissADME: a free web tool to evaluate pharmacokinetics, drug-likeness and medicinal chemistry friendliness of small molecules. Sci Rep. 2017;7: 42717.
45. Denizot F, Lang R. Rapid colorimetric assay for cell growth and survival: modifications to the tetrazolium dye procedure giving improved sensitivity and reliability. J Immunol Methods. 1986;89(2):271–277.
46. Hamdi A, Elhusseiny WM, Othman DIA, Haikal A, Bakheit AH, El-Azab AS, Al-Agamy MHM, Abdel-Aziz AA-M. Synthesis, antitumor, and apoptosis-inducing activities of novel 5-arylidenethiazolidine-2,4-dione derivatives: histone deacetylases inhibitory activity and molecular docking study. Eur J Med Chem. 2022;244:114827.
47. Sofan MA, El-Mekabaty A, Hasel AM, Said SB. Synthesis, cytotoxicity assessment and antioxidant activity of some new thiazol-2-yl carboxamides. J Heterocycl Chem. 2021;58(8): 1645–1655.
48. El-Mawgoud HK, Fouda AM, El-Nassag MA, Elhenawy AA, Alshahrani MY, El-Agrody AM. Discovery of novel rigid analogs of 2-naphthol with potent anticancer activity through multi-target topoisomerase I & II and tyrosine kinase receptor EGFR & VEGFR-2 inhibition mechanism. Chem Biol Interact. 2022;355:109838.
49. Elimam DM, Elgazar AA, El-Senduny FF, El-Domany RA, Badria FA, Eldehna WM. Natural inspired piperine-based ureas and amides as novel antitumor agents towards breast cancer. J Enzyme Inhib Med Chem. 2022;37(1):39–50.
50. Böhm H-J. Prediction of binding constants of protein ligands: a fast method for the prioritization of hits obtained from de novo design or 3D database search programs. J Comput Aided Mol Des. 1998;12(4):309–323.
51. Kramer B, Rarey M, Lengauer T. Evaluation of the FLEXX incremental construction algorithm for protein–ligand docking. Proteins. 1999;37(2):228–241.
52. Studio DJAISD, CA, USA. version 2.5; 2009.
53. DeLano WL. Pymol: an open-source molecular graphics tool. CCP4 Newsl. Protein Crystallogr. 2002;40(1):82–92.